CONTENT

Vol. 10. No. 4-2024

Published bi-monthly since 2015

ISSN 2664-0678 (Online)
ISSN 2664-066X (Print)

Publisher
Institute of Radio and Information Systems (IRIS), Vienna, Austria

Address:
1010 Wien, Austria, Ebendorferstrasse 10/6b
media-publisher.eu/synchroinfo-journal

SYNCHROINFO JOURNAL

www.media-publisher.eu/synchroinfo-journal

PHASE SHIFTERS AND ATTENUATORS IMPLEMENTATION FOR ACTIVE TRANSMITTER SIGNAL CANCELLATION IN THE RECEIVING PATH FOR SDR

Oleg Varlamov[1],

[1] Institute of Radio and Information Systems (IRIS), Vienna, Austria;

ovarlamov@media-publisher.eu

https://orcid.org/0000-0002-3996-9156

ABSTRACT

Many wideband duplex SDR applications do not use a receiver (RX) bandpass filter, so the low-noise amplifier (LNA) in the receive path must have a higher dynamic range, which comes with an increase in power consumption. To solve this problem, active transmitter signal cancellation in the receive path is used. These capabilities are considered for 5G New Radio Wireless Transceivers, for Multiple Input Multiple Output (MIMO) systems and radar applications. Solutions for the implementation of individual units, such as a delay line, digital applications, including in conjunction with analog, for various radio wave propagation channels and using neural networks are actively considered in modern literature. This paper considers options for implementing phase shifters and attenuators required for this device. The simulation of the considered implementation options for phase shifters and attenuators examples showed that the resistive digital step attenuator with a switch on MOSFETs and the attenuator on P-I-N diodes are not recommended for implementing the attenuator and phase shifter blocks of the compensation circuit. Active digital step MOS attenuator based on weighted current summation has a good dynamic range, but the output noise level seems too high over the entire possible current range. Therefore, this circuit needs noise optimization to be proposed for practical implementation. Active digital step MOS attenuator based on the composition of weighted current sources has intermodulation distortions less than –40 dB, a small parasitic phase shift and a low noise level. The high dynamic range allows installing a fixed attenuator and further reducing the output noise.

KEYWORDS: *SDR, phased antenna arrays, software-defined radio systems, Multiple Input Multiple Output, phase shifters, attenuators*

DOI: 10.36724/2664-066X-2024-10-4-2-13

Received: 12.06.2024
Accepted: 20.07.2024

Citation: Oleg Varlamov, "Phase shifters and attenuators implementation for active transmitter signal cancellation in the receiving path for SDR" *Synchroinfo Journal* **2024**, vol. 10, no. 4, pp. 2-13

1 Introduction

Phase shifters and controlled attenuators are actively used in a large number of devices from HF to microwave frequency ranges. Traditionally, controlled attenuators were used as gain control elements of receiving paths, including at the input of the device to avoid its overload with powerful signals. Currently, phase shifters and controlled attenuators are widely used in the electronic formation of phased antenna arrays (PAA) radiation patterns, determining the direction of electromagnetic radiation sources (radio direction finding), as well as in the circuitry of active transmitter signal cancellation in the receiving path for software-defined radio systems (SDR).

Since many wideband duplex SDR applications do not use a receiver (RX) bandpass filter, the low-noise amplifier (LNA) of the receive path must have a larger dynamic range, which is accompanied by an increase in power consumption. To solve this problem, active transmitter signal cancellation in the receive path is used [1, 2]. These capabilities are considered for 5G New Radio Wireless Transceivers [3], for Multiple Input Multiple Output (MIMO) systems [4] and radar applications [5]. Solutions for the implementation of individual nodes, such as a delay line, are considered in [6]. Digital applications are studied in [7-9], including jointly with analog [10], for various distribution radio wave propagation channels [11] and using neural networks [12]. Some options for active transmitter signal cancellation in the receiving path for SDR are considered by the authors in [13]. In this paper, the options for implementing phase shifters and attenuators necessary for this device are considered.

2 Phase Shifter

One of the best ways to organize the phase shift with additional attenuation can be the use of simple programmable attenuators in the signal channels with a phase shift of 90 degrees between them, as shown in Figure 1. To ensure good phase matching, all 4 programmable attenuators must be matched with each other. To reduce the number of attenuators, the following can be proposed: the phase shift is performed for the signal from one end, and the final conversion to the differential interface is performed inside an additional phase splitter, as shown in Figure 2.

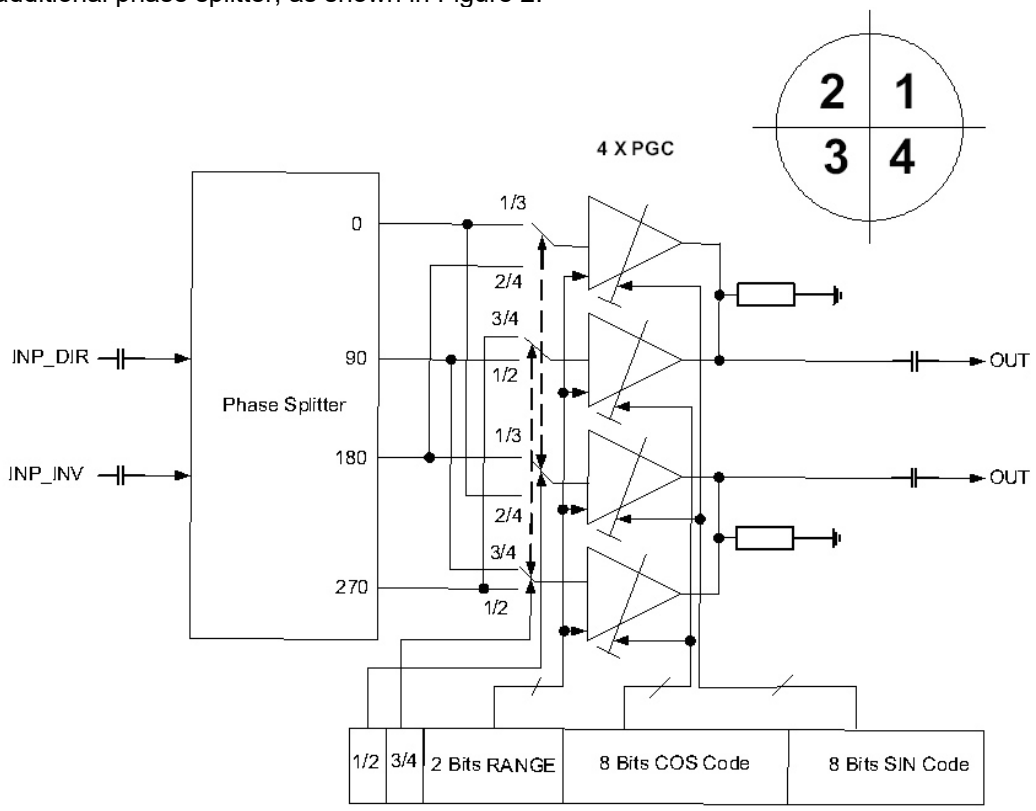

Fig. 1. Implementation of a phase shifter with 4 attenuators

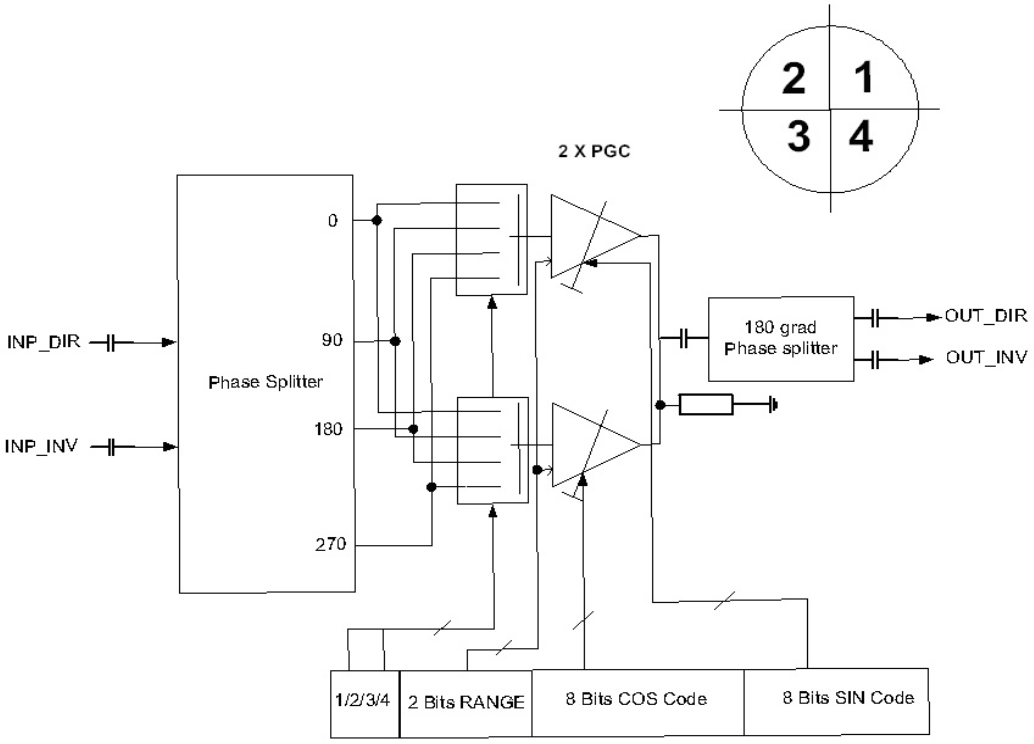

Fig. 2. Implementation of a phase shifter with 2 attenuators and a phase splitter

In the latter case, two attenuators can be very well matched.

A practical implementation of a phase splitter from a differential to a 4-phase signal is shown in Figure 3. The proposed phase splitter is well known and works well for wideband signals. The simulation results for the proposed phase splitter are shown in Figure 4.

Opportunities for improvement exist in all income groups. Low-income economies should focus on Internet access, mobile broadband penetration, and affordability. Middle- and high-income economies need to improve mobile broadband penetration and traffic per subscription.

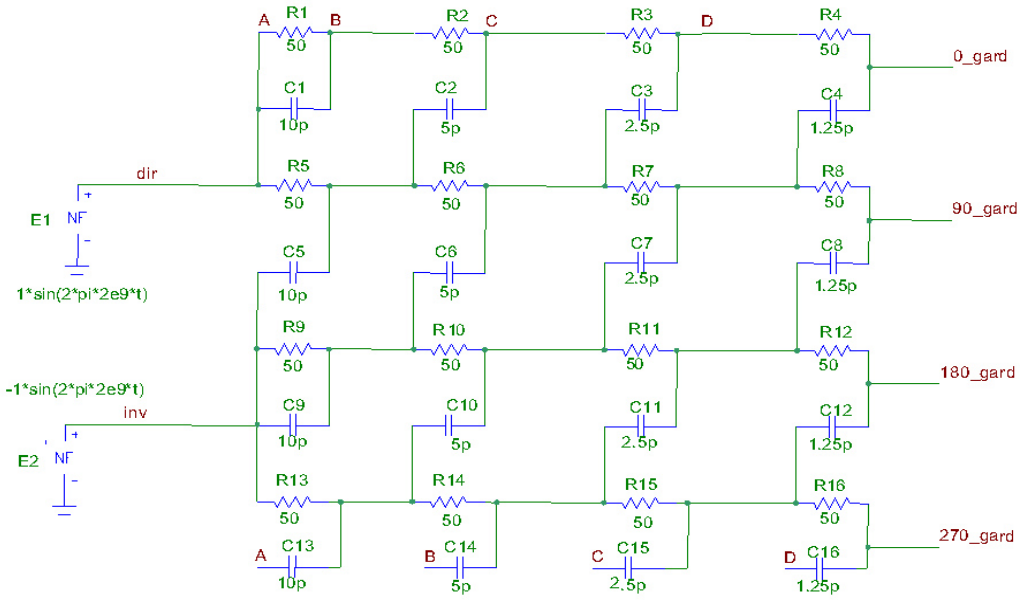

Fig. 3. Schematic implementation of a phase splitter from a differential to a 4-phase signal

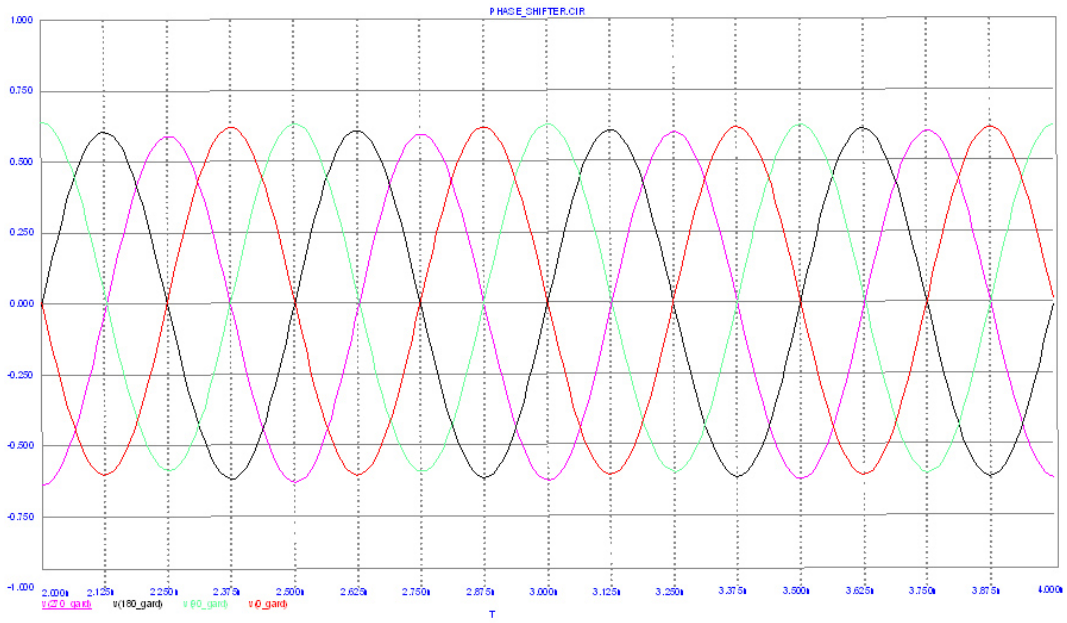

Fig. 4. Simulation results for the phase splitter

The following circuit can be proposed to convert the signal after phase shifting and attenuation to a differential output (Figure 5). Recommendations for the implementation of programmable attenuators are described in the following chapters.

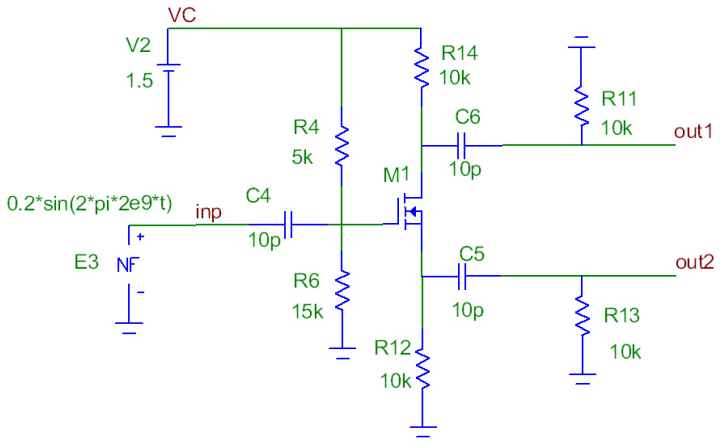

Fig. 5. Converter to differential output signals

3 Attenuator circuit implementation Examples

To implement the "Attenuator" and "Phase Shifter" blocks of the compensation circuit, an attenuator with a low noise level and a small parasitic phase shift when changing attenuation is required. Let us consider a resistive digital step attenuator, a P-I-N diode attenuator, and an active digital step MOS attenuator.

3.1 Resistive digital step attenuator.

A low-noise passive resistive digital step attenuator with a switch on MOS transistors (like the Microwave Office model) is shown in Fig. 6. The MOS transistor switch is considered as a combination of an ideal switch, an open-state resistor, and a parasitic output capacitor. The MOS transistor switches are ranked with the required resistance. The ratio of the on-resistance to the parasitic output capacitance is constant for all switches and equals 40 (example: R_{on} = 5 Ohm, C_{par} = 0.4 pF, X_{cpar} = 200 Ohm at 2 GHz). This ratio is modern for MOS technology.

The classic equation of the PI attenuator, allowing to calculate the resistance of parallel (R_{par}) and series (R_{ser}) elements:

$$R_{par} = R(A+1)/(A-1)$$

$$R_{ser} = R(A^2-1)/2A$$

where $A = U_{in}/U_{out}$ is the ratio of the input and output voltages.

To minimize the influence of switches parasitic parameters, some adjustments to the classic equation were used (after modeling and optimization):

R*par = 0.763*Rpar; Rsw_par = Rpar/5.8; R*ser = 1.218*Rser; Rsw_ser = Rser/21.1.

The results of the attenuation and parasitic phase shift analysis of the passive resistive digital step attenuator with a switch on MOSFETs are shown in Figure 7. The resistive digital step attenuator with a switch on MOSFETs has precision attenuation, but also has a large parasitic phase shift – more than 60 degrees. This circuit is not recommended for implementing the Attenuator and Phase Shifter blocks of the compensation circuit.

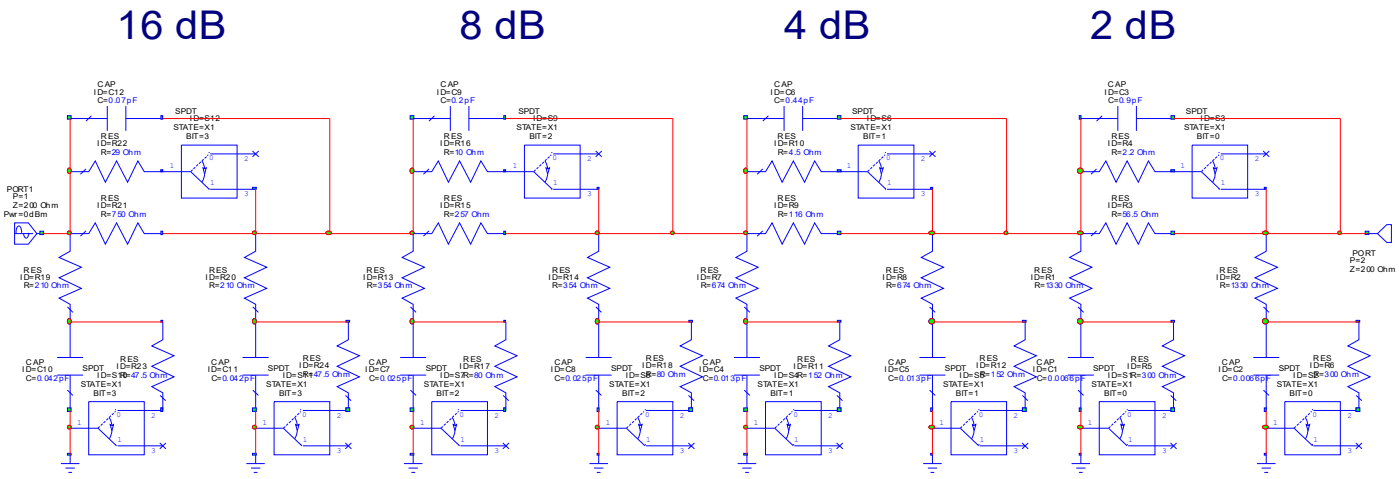

Fig. 6. Resistive digital step attenuator with a switch on MOSFETs (Microwave Office model)

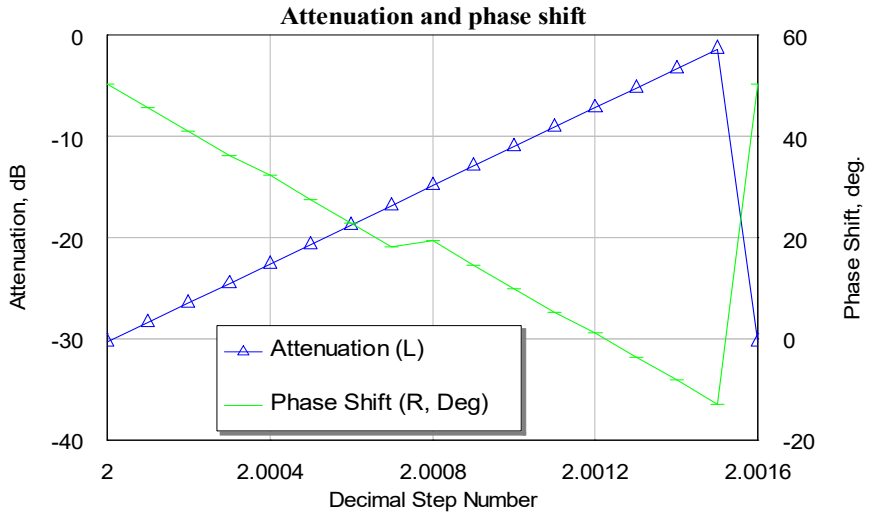

Fig. 7. Attenuation and parasitic phase shift of the passive resistive digital step attenuator with a switch on MOSFETs

3.2 P-I-N diode attenuator

The attenuator circuit based on a passive P-I-N diode [14] with a low noise level (as the Microwave Office model) is shown in Figure 8. PINDRC was used as an implementation of the Caverly PIN diode model. This advanced model is recommended for all types of PIN diode circuit design.

The equivalent circuit of the model is shown in Figure 9. The default parameters (Table 1) were used. The result of the analysis is shown in Figure 10.

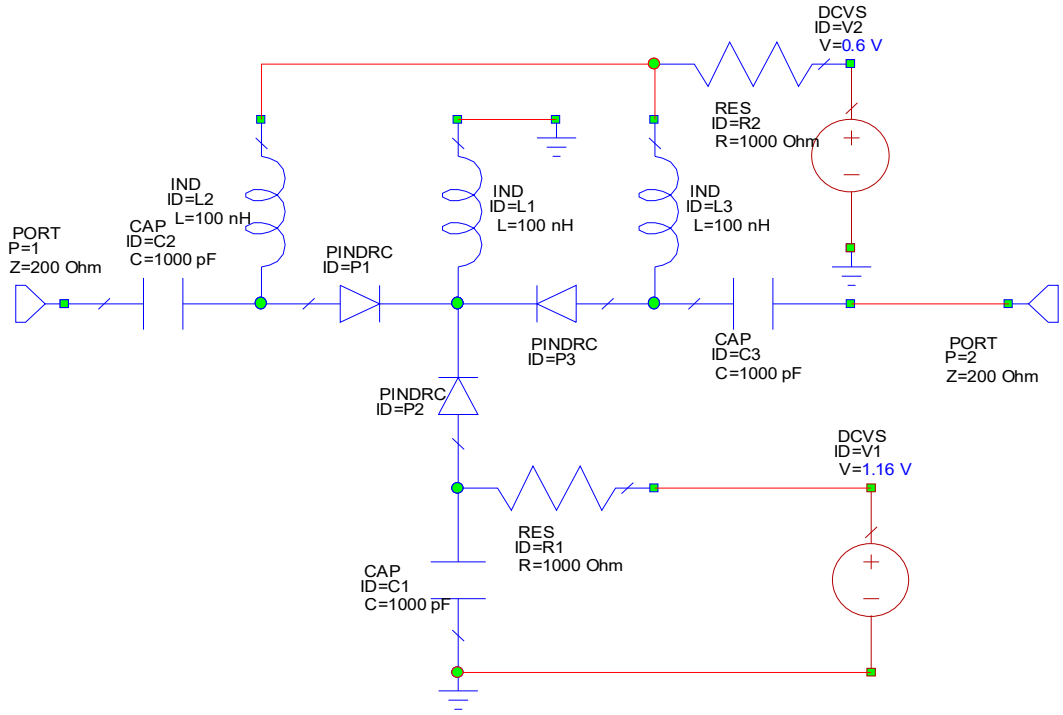

Fig. 8. P-I-N diode attenuator circuit (Microwave Office model)

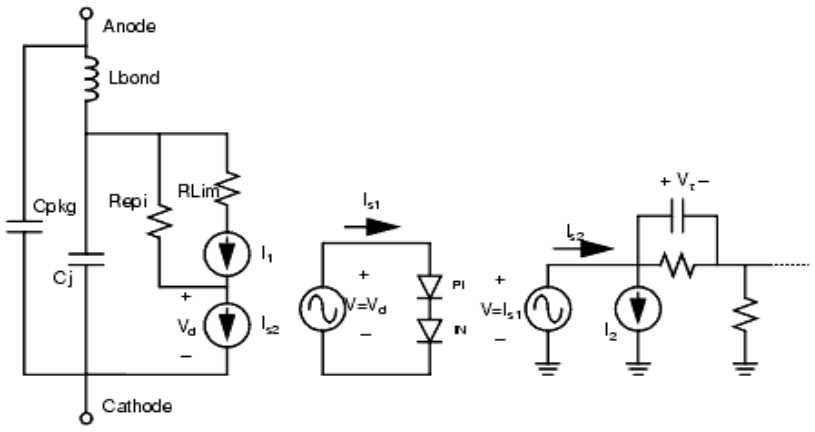

Fig. 9. Equivalent circuit of the PIN diode model

Table 1

PIN diode model parameters

Name	Description	Unit Type	Default
ID	Device ID	Text	P1
IS	Reverse saturation current	Current	1e-6 mA
IKNEE	Knee param for current dependent tau	Current	1e6 mA
N	Ideality factor	Scalar	1
RLIM	Minimum series resistance	Resistance	0.001 Ohm
REPI	Epi leakage resistance	Resistance	1000 Ohm
CJ	Reverse capacitance	Capacitance	0.1 pF
CPKG	Package capacitance	Capacitance	0.1 pF
TAU	Storage time	Time	57 ns
W	I region width in micrometers	None	6.0 mm
B	Ratio of electron to hole mobility	Scalar	3.0
LBOND	Bond wire inductance	Indictance	0.1 nH

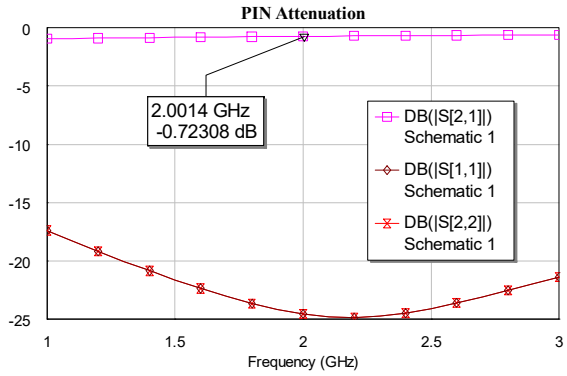

Minimum attenuation

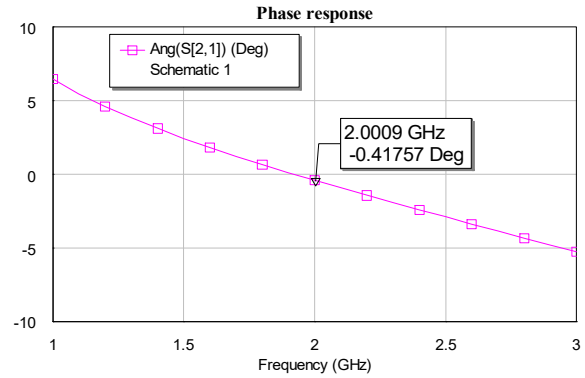

Phase response at minimum attenuation

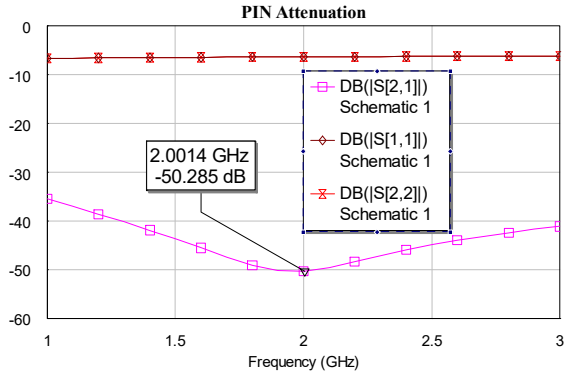

Maximum attenuation

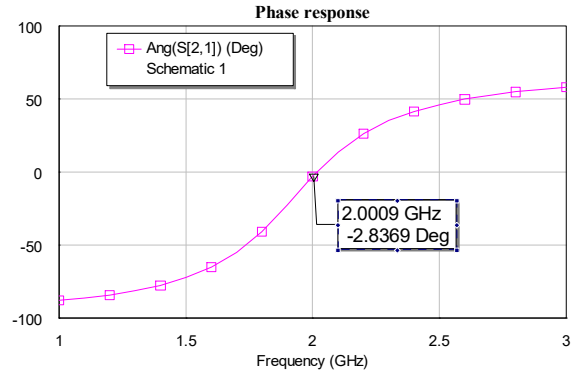

Phase response at maximum attenuation

Fig. 10. Attenuator circuit on P-I-N diodes analysis results

The attenuator on P-I-N diodes has a wide attenuation range. For zero phase shift at any attenuation, precise matching of the current in the series and shunt path is required. The total current for all P-I-N diodes is about 4 mA at any attenuation - this is too much for the compensation circuit. Therefore, this circuit also cannot be recommended for implementing the Attenuator and Phase Shifter blocks of the compensation circuit.

3.3 Active digital step MOS attenuator

Two versions of the active step MOS attenuator are developed and considered. The first structure, shown in Figure 11, is based on the composition of weighted current sources. The four-bit part of the active digital step attenuator with the inclusion of MOS transistors is shown in Figure 11. The radio frequency signals from the resistive prescaler R1…R4 control four current generators implemented on NMOS transistors M1…M4 and resistors R18…R21. This allows to reduce the dynamic range of the scaling resistors. Thus, for an 8-bit attenuator, the range of resistor values is 16 instead of 256 without a prescaler. The output signal level is determined by NMOS switches in the sources of transistors M1…M4. Capacitors C17…C21 are installed to compensate for the parasitic phase shift. The power consumption of this circuit directly depends on the output signal level.

Since the real transistor model is not defined, a simplified model was used. The model includes nonlinear and noise characteristics of the transistor, but does not take into account the frequency characteristics. Therefore, the circuit shown in Figure 12 was used for the analysis.

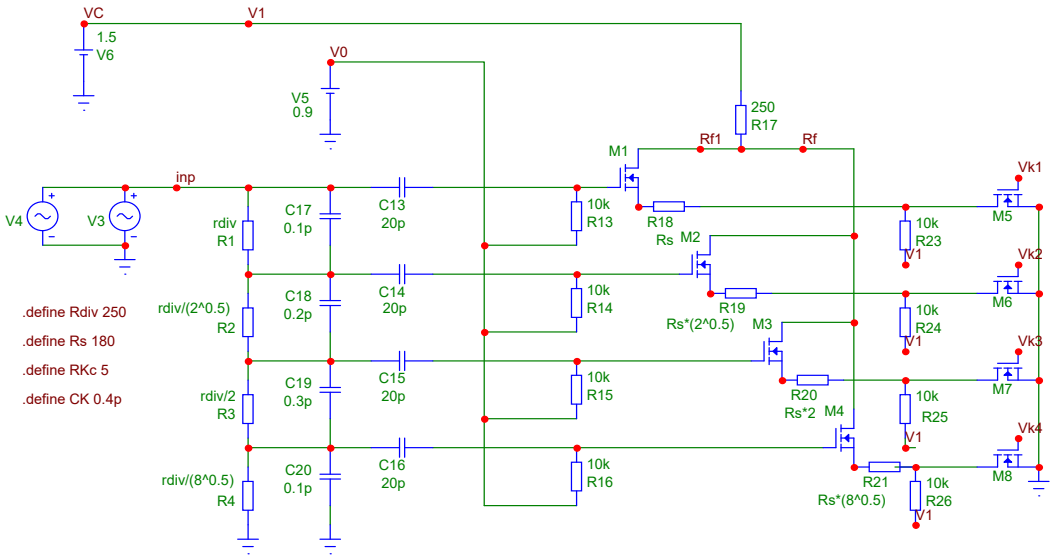

Fig. 11. Active digital step attenuator circuit (4-bit part)

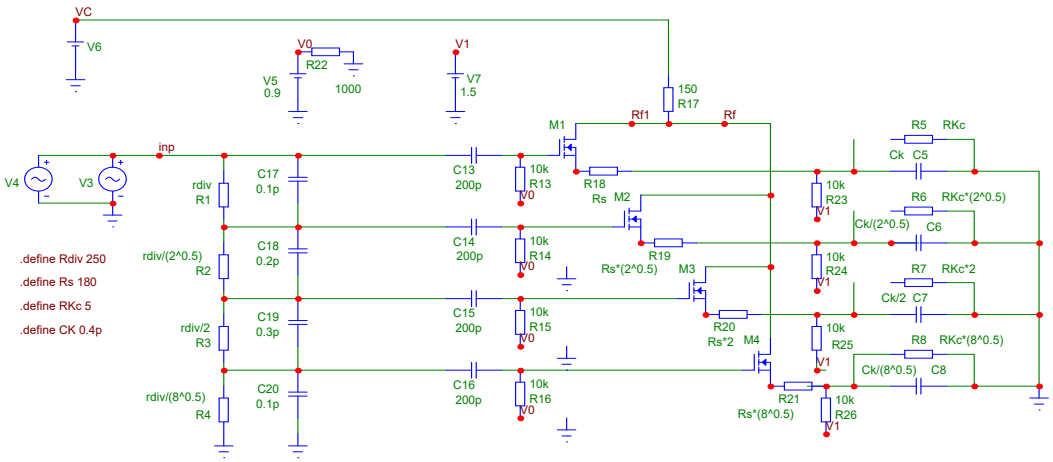

Fig. 12. Active digital step attenuator circuit model (4-bit part)

The real switches are represented by ideal switch with linear resistance and capacitance (R5…R8, C5…C8). The analysis results are shown in Fig. 13…16. The circuit has intermodulation distortions less than –40 dB on a two-tone test signal. The analyzed attenuator has a small parasitic phase shift and a low noise level. The high dynamic range allows installing a fixed attenuator and further reducing the output noise.

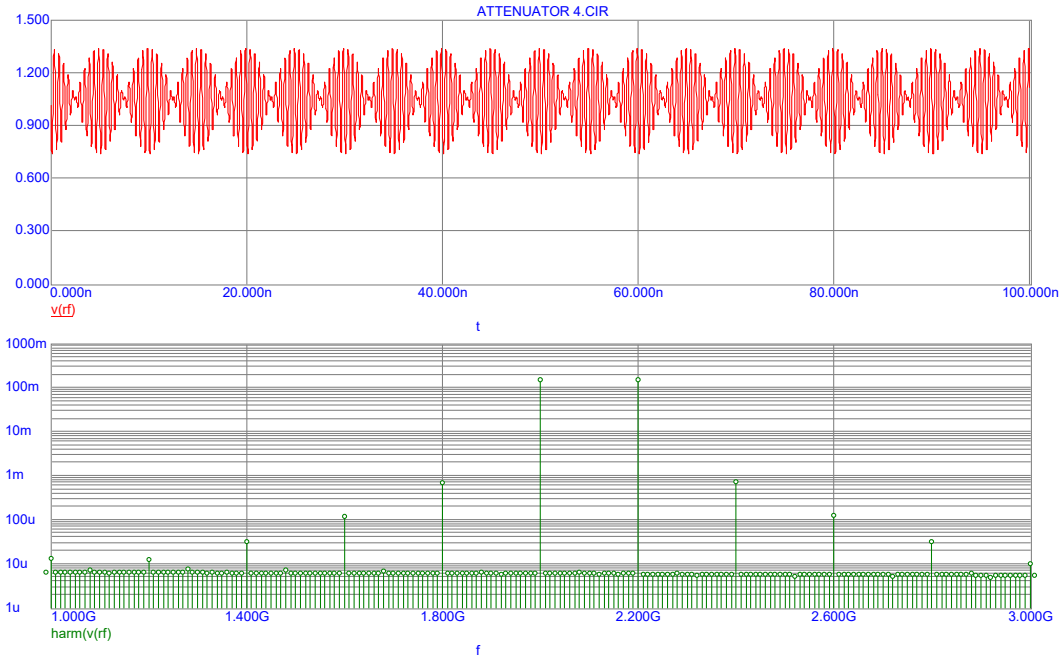

Fig. 13. Transient analysis result. Minimum attenuation

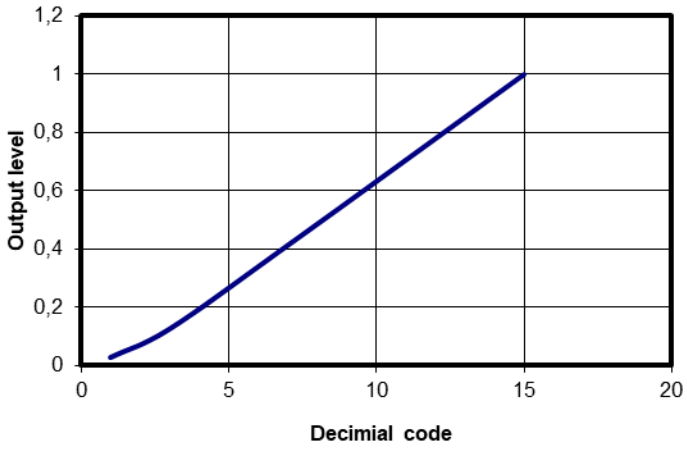

Fig. 14. Attenuator response

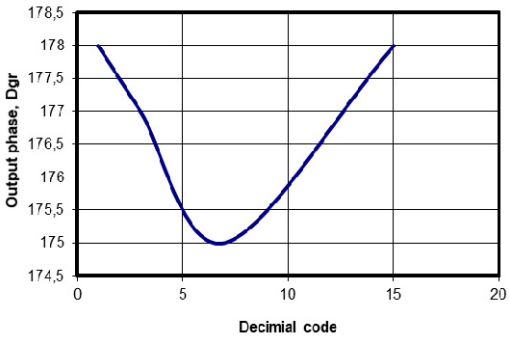

Fig. 15. Parasitic phase shift of the attenuator

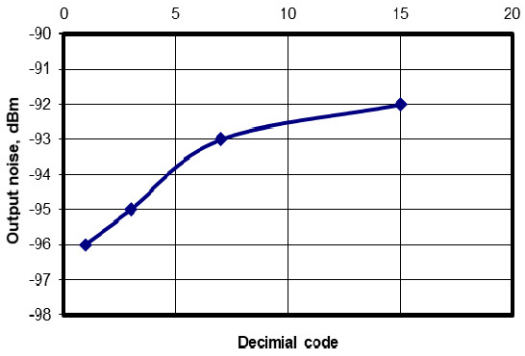

Fig. 16. Attenuator output noise, recalculated for a 50 ohm load

The second structure, shown in Figure 17, is based on weighted current summation. Switched current generators M3…M10 have different sizes based on the binary code. Switched transistors installed in the gate paths of the output transistors can be very small. Switched load resistors determine the scale range of the attenuator. The analysis results for this circuit are shown in Figures 18, 19. As can be seen, the circuit has a good dynamic range, but the output noise level seems too high over the entire possible current range. Therefore, this circuit needs noise optimization to be proposed for practical implementation.

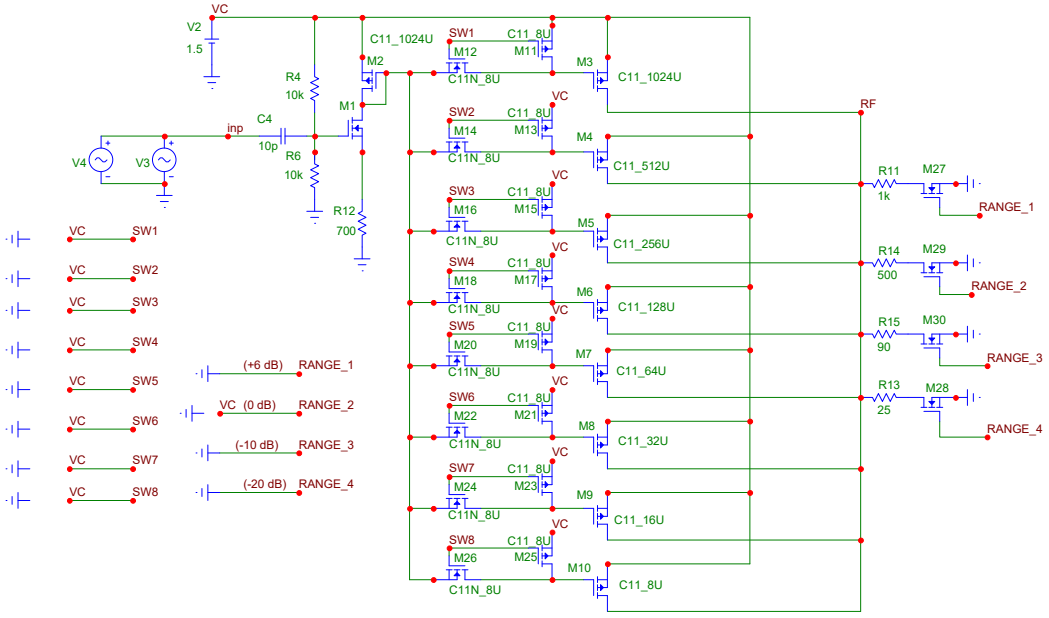

Fig. 17. Attenuator based on current summation

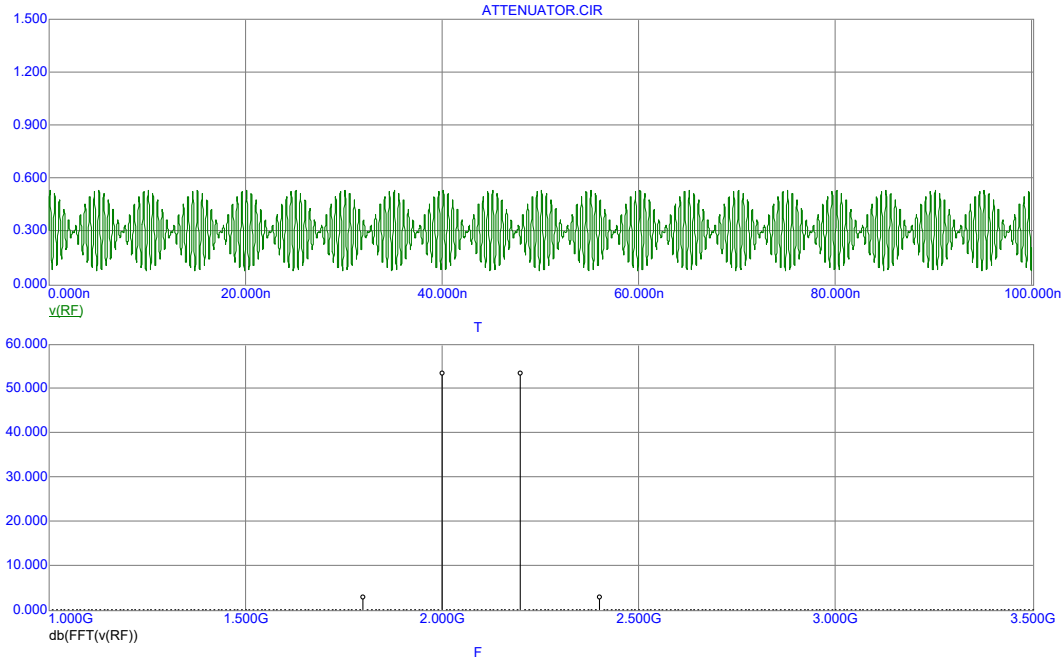

Fig. 18. Transient analysis result. Minimum attenuation

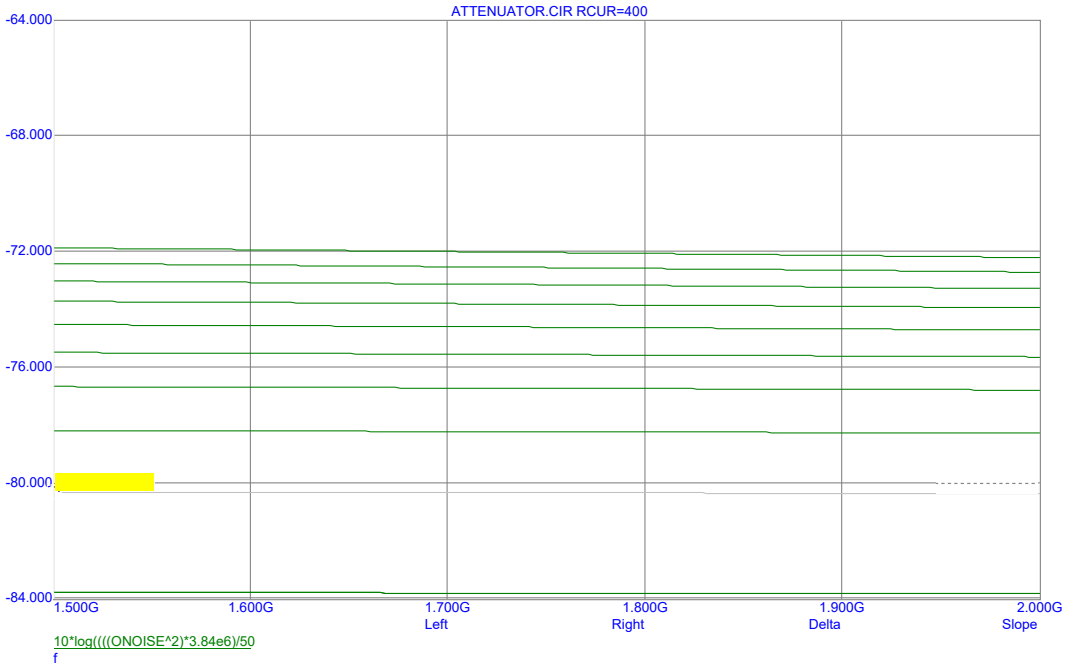

Fig. 19. Output noise power versus current control resistor value

Conclusion

The simulation of the considered implementation options for phase shifters and attenuators examples showed that:

– The resistive digital step attenuator with a switch on MOSFETs has precision attenuation, but also has a large parasitic phase shift – more than 60 degrees;

– The attenuator on P-I-N diodes has a wide attenuation range. For zero phase shift at any attenuation, precise matching of the current in the series and shunt path is required. The total current for all P-I-N diodes is about 4 mA at any attenuation – this is too much for the compensation circuit;

Both these circuits are not recommended for implementing the attenuator and phase shifter blocks of the compensation circuit.

– Active digital step MOS attenuator based on weighted current summation has a good dynamic range, but the output noise level seems too high over the entire possible current range. Therefore, this circuit needs noise optimization to be proposed for practical implementation;

– Active digital step MOS attenuator based on the composition of weighted current sources has intermodulation distortions less than –40 dB, a small parasitic phase shift and a low noise level. The high dynamic range allows installing a fixed attenuator and further reducing the output noise.

REFERENCES

[1] J. Zhou, A. Chakrabarti, P. R. Kinget and H. Krishnaswamy, "Low-Noise Active Cancellation of Transmitter Leakage and Transmitter Noise in Broadband Wireless Receivers for FDD/Co-Existence," *IEEE Journal of Solid-State Circuits*, vol. 49, no. 12, pp. 3046-3062, Dec. 2014, doi: 10.1109/JSSC.2014.2359914.

[2] L. Laughlin et al., "Tunable Frequency-Division Duplex RF Front End Using Electrical Balance and Active Cancellation," *IEEE Transactions on Microwave Theory and Techniques*, vol. 66, no. 12, pp. 5812-5824, Dec. 2018, doi: 10.1109/TMTT.2018.2851990.

[3] S. Sadjina, C. Motz, T. Paireder, M. Huemer and H. Pretl, "A Survey of Self-Interference in LTE-Advanced and 5G New Radio Wireless Transceivers," *IEEE Transactions on Microwave Theory and Techniques*, vol. 68, no. 3, pp. 1118-1131, March 2020, doi: 10.1109/TMTT.2019.2951166.

[4] Y. Cao and J. Zhou, "Integrated Self-Adaptive and Power-Scalable Wideband Interference Cancellation for Full-Duplex MIMO Wireless," *IEEE Journal of Solid-State Circuits*, vol. 55, no. 11, pp. 2984-2996, Nov. 2020, doi: 10.1109/JSSC.2020.3005755.

[5] J. Zhang, Z. Zhang, Y. Li, C. Gu and J. Mao, "Target Detection with Short-Range FMCW Radar Based on Time-Frequency Characteristic-Based Leakage Cancellation Technique," *IEEE Transactions on Microwave Theory and Techniques*, doi: 10.1109/TMTT.2024.3360324.

[6] A. Nagulu et al., "A Full-Duplex Receiver with True-Time-Delay Cancelers Based on Switched-Capacitor-Networks Operating Beyond the Delay–Bandwidth Limit," *IEEE Journal of Solid-State Circuits*, vol. 56, no. 5, pp. 1398-1411, May 2021, doi: 10.1109/JSSC.2021.3063658.

[7] L. Anttila et al., "Full-Duplexing with SDR Devices: Algorithms, FPGA Implementation, and Real-Time Results," *IEEE Transactions on Wireless Communications*, vol. 20, no. 4, pp. 2205-2220, April 2021, doi: 10.1109/TWC.2020.3040226.

[8] S. Song et al., "Digital Self-Interference Cancellation with Robust Multi-layered Total Least Mean Squares Adaptive Filters," *2023 IEEE 98th Vehicular Technology Conference (VTC2023-Fall)*, Hong Kong, Hong Kong, 2023, pp. 1-5, doi: 10.1109/VTC2023-Fall60731.2023.10333436.

[9] J. Tamminen et al., "Digitally-controlled RF self-interference canceller for full-duplex radios," *2016 24th European Signal Processing Conference (EUSIPCO)*, Budapest, Hungary, 2016, pp. 783-787, doi: 10.1109/EUSIPCO.2016.7760355.

[10] X. Huang, A. Tuyen Le and Y. J. Guo, "Joint Analog and Digital Self-Interference Cancellation for Full Duplex Transceiver with Frequency-Dependent I/Q Imbalance," *IEEE Transactions on Wireless Communications*, vol. 22, no. 4, pp. 2364-2378, April 2023, doi: 10.1109/TWC.2022.3211316.

[11] A. Kurt, M. B. Salman, U. B. Sarac and G. M. Guvensen, "An Adaptive-Iterative Nonlinear Interference Cancellation in Time-Varying Full-Duplex Channels," *IEEE Transactions on Vehicular Technology*, vol. 72, no. 2, pp. 1862-1878, Feb. 2023, doi: 10.1109/TVT.2022.3208766.

[12] M. H. Attar et al., "Towards Adaptive Digital Self-Interference Cancellation in Full-Duplex Wireless Transceivers: APSM vs. Neural Networks," *2022 56th Asilomar Conference on Signals, Systems, and Computers*, Pacific Grove, CA, USA, 2022, pp. 1223-1227, doi: 10.1109/IEEECONF56349.2022.10052049.

[13] Grigory Itkin, Oleg Varlamov, "Active transmitter signal cancellation in receive signal path for SDR," *Synchroinfo Journal*, 2024, vol. 10, no. 1, pp. 8-17.

[14] O.V. Varlamov "Maximum power of the HF antenna tuner switched by PIN diodes at load mismatch," T-Comm, 2020, vol. 14, no.10, pp. 26-32. doi: 10.36724/2072-8735-2020-14-10-26-32.

SYNCHROINFO JOURNAL

www.media-publisher.eu/synchroinfo-journal

WIND INFLUENCE ON THE POLLUTANTS EMITTED SPREAD BY MOTOR VEHICLES

Tofik I. Suleymanov, Shamsi E. Mamedov[1], Elshan R. Ragimov[2], Jeyhun R. Rahimov[3],

[1] Azerbaijan National Aerospace Agency, Baku, Azerbaijan;

[2] Baku Higher Oil School, Baku, Azerbaijan;

[3] Azerbaijan Technical University, Baku, Azerbaijan

ABSTRACT

The known static and dynamic wind speed influence models on the urban air purification degree from CO emitted by urban transport are analyzed. Three optimization problems of adaptive motor transport traffic organization of are formulated and solved on the dynamic model. It is proposed to introduce a control function for the total emitted amount of wind speed CO depending. The optimal function type is calculated, at which the pollutant rise height reduced to a minimum. The solution of the second optimization problem made it possible to determine those most unfavorable conditions, at which the safe distance to highway for a nearby settlement can reach a maximum. As a result of solving the third optimization problem, it is shown that the minimum average value of CO concentration at a certain height can be achieved with a certain dependence of wind speed horizontal component on the height of point under consideration.

DOI: 10.36724/2664-066X-2024-10-4-14-20

Received: 10.07.2024
Accepted: 06.08.2024

Citation: T.I. Suleymanov, Sh.E. Mamedov, E.R. Ragimov, J.R. Rahimov, "Wind influence on the pollutants emitted spread by motor vehicles" *Synchroinfo Journal* **2024**, vol. 10, no. 4, pp. 14-20

Licensee IRIS, Vienna, Austria.

KEYWORDS: *motor transport, dynamic model, air pollutant, adaptive control, optimization*

1 Introduction

As noted in [1], currently 55% of the world's population lives in cities and by 2050 this figure will increase to 68%. Rapid urbanization has led to the fact that only 12% of city dwellers live in areas where air quality meets the requirements of the World Health Organization. Pollution of urban areas largely depends on the correct planning of urban development and taking into account such a natural factor of urban air purification as wind. As noted in [2-5], the distribution of air pollutants largely depends on the characteristics of the air flow in the urban environment.

At the same time, the problem of urban air pollution should be solved by proper planning of the urban transport network, taking into account the development and placement of densely populated areas. It is well known that the main air pollutants emanating from vehicles are CO, SO2, NO2 and aerosols. At the same time, the most potent of them on living organisms is carbon monoxide (CO). The study of the effect of wind on the spread of these pollutants to the level of permitted standards, carried out in [1], showed that under conditions of static wind, i.e. at constant wind speed, the decrease in pollutant concentration can be expressed as a decreasing exponential function of time

$$y = a_1 \exp(-a_2 t) \tag{1}$$

where a_1, a_2 are model indicators depending on wind speed; t is time. At the same time, it is obvious that wind speed is a dynamic parameter, which leads to the need to take this factor into account. In this regard, the most effective approach to solving this problem can be considered the mathematical model developed in the work [6], which took into account such indicators as CO emissions from the urban transport network, average atmospheric temperature, wind speed, traffic flow intensity, maximum permissible concentration of pollutants for the human body, and other indicators. Note that in many studies [7-10].

CO is indicated as the main air pollutant from vehicles, the maximum concentration of which is 10 mg/m^3 for 8 hours. According to the work [6], taking into account C = 0.01 g/m^3, the minimum safe distance Dmin between the highway and the settlement can be expressed through the standard deviations of the pollutant level along the coordinates y and

$$z\sigma_y = 0{,}32 D_{min} \tag{2}$$

$$\sigma_z = 0{,}24 D_{min} \tag{3}$$

In this case, Dmin is determined by the expression [6]

$$D_{min} = \frac{k\Delta h^{1/2} Q^{1/4}}{U^{1/4}} \tag{4}$$

where Δh is the elevation (lift) distance of the pollutant (m); U is the wind speed; h is the total volume of CO emissions from motor vehicles; k is the coefficient depending on the model parameters.

Note that formula (4) obtained in [6] allows us to formulate the following problems: (1) for a given D_{min}, how should the Q parameter be controlled depending on the current wind speed in order to achieve the minimum value of Δh; (2) for a given Δh, how should the Q parameter be controlled in order to obtain the minimum value of D_{min} (3) determining the average value of Dmin taking into account the altitude distribution of wind speed, i.e. the function $U = U(\Delta h)$.

Materials and methods

Let us consider the possibility of solving the first problem. We will rewrite expression (4) in following form

$$\Delta h = \frac{D_{min}^2 U}{k^2 Q^{1/2}} \tag{5}$$

Let us introduce for consideration the function of controlling the degree of CO emission, i.e. the indicator *Q* depending on the wind speed *U*, i.e.

$$Q = f(U) \tag{6}$$

Note that the control of *Q* indicator can be implemented by prohibiting the entry of heavy-duty transit vehicles and passing them along bypass routes at low wind speeds. Taking into account (5) and (6), we obtain

$$\Delta h = \frac{D_{min}^2 U}{k^2 \sqrt{f(U)}} \tag{7}$$

Since, unlike the model proposed in [1], we are considering a dynamic model of wind impact, we will consider the case when, over a period of time Δt, the wind speed increases from zero to U_{max}. Consequently, the average value Δh is determined as

$$\Delta h_{cp} = \frac{1}{U_{max}} \int_0^{U_{max}} \frac{D_{min}^2 U}{k^2 \sqrt{f(U)}} dU \tag{8}$$

To solve the problem of determining the optimal function *f*(*U*), we impose the following restrictive condition on this function

$$\int_0^{U_{max}} f(U)\, dU = C_1;\ C_1 = const \tag{9}$$

Taking into account expressions (8) and (9), we will form the target functional of unconditional variational optimization

$$F_1 = \frac{1}{U_{max}} \int_0^{U_{max}} \frac{D_{min}^2 U}{k^2 \sqrt{f(U)}} dU + \lambda_1 \left[\int_0^{U_{max}} f(U)\, dU - C_1 \right] \tag{10}$$

where λ is the Lagrange multiplier.

Solution to optimization problem (10) according to [11] must satisfy the condition

$$\frac{d\left\{ \frac{D_{min}^2 U}{U_{max} k^2 \sqrt{f(U)}} + \lambda_1 f(U) \right\}}{df(U)} = 0 \tag{11}$$

From condition (11)

$$-\frac{1}{2} \frac{D_{min}^2 U}{U_{max} k^2 f(U)^{3/2}} + \lambda_1 = 0 \tag{12}$$

From expression (12)

$$f(U) = \sqrt[3]{\frac{D_{min}^2 U^2}{4\lambda_1^2 k^4}} \quad (13)$$

when solving (13), F_1 reaches a minimum, since expression (12) always has a positive derivative with respect to $f(U)$. To calculate the value of λ, we can use formulas (9) and (13). We have

$$\int_0^{U_{max}} \sqrt[3]{\frac{D_{min}^2 U^2}{4\lambda_1^2 k^4}}\, dU = C_1 \quad (14)$$

From expression (14)

$$\sqrt[3]{4\lambda_1^2} = \frac{1}{C_1} \int_0^{U_{max}} \sqrt[3]{\frac{D_{min}^3 U^2}{k^4}}\, dU \quad (15)$$

From expression (15)

$$\lambda_1 = \frac{1}{4}\left[\frac{1}{C_1} \int_0^{U_{max}} \sqrt[3]{\frac{D_{min}^3 U^2}{k^4}}\, dU\right]^{3/2} \quad (16)$$

Let us consider the possibility of solving the second problem mentioned above. Taking into account expressions (4) and (6), we will form the following functional

$$D_{min.cp} = \frac{1}{U_{max}} \int_0^{U_{max}} \frac{\Delta h k^2 f(U)^{1/2}}{U}\, dU \quad (17)$$

To calculate the optimal function $f(U)$, we use the restrictive condition (9). Taking into account expressions (17) and (9), we form the following objective functional

$$F_2 = \frac{1}{U_{max}} \int_0^{U_{max}} \frac{\Delta h k^2 f(U)^{1/2}}{U} + \lambda_2 \left[\int_0^{U_{max}} f(U)\, dU - C_1\right] \quad (18)$$

where λ_2 is the Lagrange multiplier.

The solution to problem (18) must satisfy condition

$$\frac{d\left\{\frac{\Delta h k^2 f(U)^{1/2}}{U_{max} U} + \lambda_2 f(U)\right\}}{df(U)} = 0 \quad (19)$$

From condition (19) we obtain

$$\frac{1}{2} \frac{\Delta h k^2}{U_{max} f(U)^{1/2} U} - \lambda_2 = 0 \quad (20)$$

From condition (20)

$$f(U) = \frac{\Delta h^2 k^4}{4 U_m^2 \lambda_2^2 U^2} \quad (21)$$

When solving (21), the functional F_2 reaches its maximum, since the derivative of expression (19) with respect to the desired function always turns out to be a negative value. To calculate λ_2, we can use expressions (9) and (21). We have

$$\int_0^{U_{max}} \frac{\Delta h^2 k^4}{4 U_m^2 \lambda_2^2 U^2}\, dU = C_1 \quad (22)$$

From condition (22)

$$\lambda_2 = \sqrt{\frac{\int_0^{U_{max}} \frac{\Delta h^2 k^4}{4U_m^2 \lambda_2^2 U^2} dU}{C_1}} \tag{23}$$

Thus, according to the solution of the second problem, the maximum average value of pollutant lift can be obtained at minimum Q and maximum wind speed. Obviously, such a regime is completely unprofitable and should be avoided.

Let us consider the solution of the third above-mentioned research problem. Next, we will study the optimal form of the function

$$U = U(\Delta h) \tag{24}$$

at which the average value D_{min} would reach its minimum value.

For the model solution of this problem, we will adopt the following restrictive condition

$$\int_0^{\Delta h_{max}} U(\Delta h) d(\Delta h) = C; C = const \tag{25}$$

Taking into account expressions (4) and (24), we define the target optimization functional as

$$F_1 = \frac{1}{\Delta h} \int_0^{\Delta h_{max}} \frac{k \Delta h^{\frac{1}{2}} Q^{\frac{1}{4}}}{U \Delta h^{\frac{1}{4}}} d(\Delta h) \tag{26}$$

Taking into account expressions (25) and (26), we will compose the objective functional F_0 of unconditional variational optimization

$$F_0 = \frac{1}{\Delta h_{max}} \int_0^{\Delta h_{max}} \frac{k \Delta h^{\frac{1}{2}} Q^{\frac{1}{4}}}{U \Delta h^{\frac{1}{4}}} d(\Delta h) + \lambda \left[\int_0^{\Delta h_{max}} U(\Delta h) d(\Delta h) - C \right] \tag{27}$$

where λ – is the Lagrange multiplier.

The solution to problem (27) according to [11] must satisfy the condition

$$\frac{d\left\{ \frac{1}{\Delta h_{max}} \frac{k \Delta h^{\frac{1}{2}} Q^{\frac{1}{4}}}{U(\Delta h)^{\frac{1}{4}}} + \lambda U(\Delta h) \right\}}{dU(\Delta h)} = 0 \tag{28}$$

From condition (28)

$$-\frac{1}{4} \frac{k \Delta h^{\frac{1}{2}} Q^{\frac{1}{4}}}{\Delta h_{max} U(\Delta h)^{\frac{5}{4}}} + \lambda = 0 \tag{29}$$

From condition (29)

$$U(\Delta h) = \frac{k^{\frac{4}{5}} h^{\frac{4}{10}} Q^{\frac{4}{20}}}{h_m \lambda} \tag{30}$$

Taking into account expressions (25) and (30), we obtain

$$\frac{k^{\frac{4}{5}}Q^{\frac{4}{20}}}{h_m\lambda}\int_0^{h_m} h^{\frac{4}{10}}dh = C \quad (31)$$

From condition (31)

$$\lambda = \frac{10}{14}\frac{k^{\frac{4}{5}}Q^{\frac{4}{20}}h_m^{\frac{4}{10}}}{Ch_m} \quad (32)$$

From expressions (30) and (32) finally obtain

$$U(\Delta h) = \frac{7}{5}\frac{C\Delta h^{\frac{2}{5}}}{h_m^4} \quad (33)$$

Thus, when condition (33) is met, the $D_{\min}$ indicator reaches a minimum on average. The fact that the minimum is reached is confirmed by the fact that the derivative of expression (29) with respect to the desired function is always a positive function.

We rewrite expression (33) as

$$U(\Delta h) = C_1 h^{\frac{2}{5}} \quad (34)$$

where

$$C_1 = \frac{7C}{5h_m^4} \quad (35)$$

Taking into account expressions (26) and (34), we calculate the minimum value of F_1 that can be achieved. We have

$$F_{1min} = \frac{1}{\Delta h_{max}}\int_0^{\Delta h_{max}} \frac{k\Delta h^{\frac{1}{2}}Q^{\frac{1}{4}}}{C_1^{\frac{1}{4}}(\Delta h)^{\frac{1}{10}}}d\Delta h = \frac{kQ^{\frac{1}{4}}}{C_1^{\frac{1}{4}}\Delta h_m}\int_0^{\Delta h_{max}} \Delta h^{\frac{4}{10}}d\Delta h = C_2\Delta h_{max}^{\frac{2}{5}} \quad (36)$$

where $C_2 = \frac{5kQ^{\frac{1}{4}}}{7C_1^{\frac{1}{4}}}$.

Discussion

The known static and dynamic models of wind speed influence on the urban air purification degree from CO emitted by urban transport are analyzed. It is noted that the known static model allows determining the time during which the concentration of CO in urban air can decrease to an acceptable level at a constant specified wind speed. A dynamic model of wind speed influence is considered, which allows calculating a safe distance to the highway at different wind speeds. Based on the dynamic model, two optimization problems are formulated and solved based on the adaptive organization of vehicle traffic. It is proposed to introduce the function $Q = f(U)$, i.e. the function of controlling the total emitted amount of CO depending on the wind speed. Physically, the implementation of such a mode means introducing a restriction for some types of transport depending on the wind speed. The optimal type of the introduced function is calculated, at which Δh to the highway decreases to a minimum.

The solution of the second optimization problem made it possible to determine an unfavorable condition for practice, under which the safe distance to the highway can reach a maximum. According to the solution of the third optimization problem, it was found that the minimum average value of CO concentration at a certain height can be achieved with a certain dependence of the wind speed horizontal component on the point under consideration height.

Key findings and conclusion

1. It was determined that static and dynamic models were developed with respect to the impact of wind speed on the degree of urban air purification, whereby the static model allows determining the air purification time, and the dynamic model allows calculating the safe distance to the highway.

2. Based on the dynamic model, two optimization problems were formulated and solved; according to the solution of the first problem, the conditions under which the height of the pollutant rise can reach a minimum were determined. According to the solution of the second problem, the most unfavorable conditions were determined under which the safe distance to the highway increases to a maximum.

3. If, under the assumptions made above, the growth of Δh is accompanied by an increase in the horizontal wind speed, then under the adopted restrictive condition, it is possible to achieve the minimum average value of CO concentration.

4. The growth of Δh max, while the previously adopted conditions remain unchanged, is accompanied by an increase in the achievable minimum average value of CO concentration.

REFERENCES

[1] L. Yan, W. Hu, M. Q. Yin, “An investigation of the correlation between pollutant dispersion and wind environment: evaluation of static wind speed,” *Pol. J. Environ. Stud*. Vol. 30. No. 5. 2021, pp. 4311-4323.

[2] H. J. S. Fernando, S. M. Lee, J. Anderson, M. Princevac, E. Pardyjak, “Grossman-Clarke, S. Urban fluid mechanics: air circulation and contaminant dispersion in cities,” *Environ. Fluid Mech*. 1, 107, 2001.

[3] Z. L. Gu, Y. W. Zhang, Y. Cheng, S. C. Lee, “Effect of uneven building layout on air flow and pollutant dispersion in non-uniform street canyons,” *Build. Environ*. 46, 2657, 2011.

[4] C. Gromke, “A vegetation modeling concept for building and environmental aerodynamics wind tunnel tests and its application in pollutant dispersion studies,” *Environ. Pollut*. 159, 2094, 2011.

[5] Y. X. Du, B. Blocken, S. Pirker, “A novel approach to simulate pollutant dispersion in the built environment: Transport-based recurrence CFD,” *Build. Environ*. 170, 1, 2020.

[6] M. Hadipour, S. Pourebrahim, A. R. Mahmmud, “Mathematical modeling considering air pollution of transportation: an urban environmental planning, case study in petaling Jaya, Malaysia,” *Theoretical and empirical researches in urban management*. No. 4(13). 2009.

[7] Clean Water Action Council, “Environmental Impacts of Transportation,” USA, 2008.

[8] G. Haughton, C. Hunter, H. Haughton, “Sustainable Cities,” Routledge publisher, UK, 2003.

[9] T. Meszaros, L. Haszpra, A. Gelencser, “Tracking Changes in Carbon Monoxide Budget over Europe between 1995 and 2000,” *Journal of Atmospheric*, 2005.

[10] J. P. Rodrigue, C. Comtois, B. Slack, “The Geography of Transport Systems,” Taylor and Francis group publisher,” USA, 2006.

[11] L. E. Elsgolts, “Differential equations and calculus of variations,” Moscow: Nauka, 2000, 424 p.

ELECTROMAGNETIC BACKGROUND GENERATED BY LOW EARTH ORBIT SATELLITES ON THE EARTH'S SURFACE

Vladimir Mordachev[1], **Dzmitry Tsyanenka**[1], **Aliaksandr Svistunou**[1], **Gang Wu**[2], **Valery Tikhvinskiy**[3],

[1] EMC R&D Lab, Belarusian State University of Informatics and Radioelectronics (BSUIR), Belarus;

mordachev@bsuir.by, tsiond@tut.by, emc@bsuir.by

[2] University of Electronic Science and Technology of China (UESTC), China;

wugang99@uestc.edu.cn

[3] Radio Research and Development Institute (NIIR), Russia;

vtniir@mail.ru

ABSTRACT

A methodology for evaluation the levels of electromagnetic background (EMB) created near the earth's surface by mega-constellations of low earth orbit satellites is proposed. Analysis of EMB levels at the earth's surface created by these satellite's mega-constellations indicate that with their full-scale deployment, the average level of artificial EMB of the SHF range at the earth's surface can exceed the average intensity of natural EMB by many orders of magnitude. Such an essential change in physical characteristics of operating electromagnetic environment for ground radio services and habitat requires serious attention and further in-depth analysis.

DOI: 10.36724/2664-066X-2024-10-4-21-30

Received: 02.07.2024
Accepted: 10.08.2024

Citation: V. Mordachev, D. Tsyanenka, A. Svistunou, Gang Wu, V. Tikhvinskiy, "Electromagnetic background generated by low earth orbit satellites on the earth's surface" *Synchroinfo Journal* **2024**, vol. 10, no. 4, pp. 21-30

Licensee IRIS, Vienna, Austria.

KEYWORDS: *low orbit satellite, electromagnetic radiation, total radiated power, electromagnetic background*

1 Introduction

The observed deployment in the near-earth space of megaconstellations of low earth orbit communication satellites (Starlink, OneWeb, Astra, Kuiper, GuoWang, etc.) will increase by 2-3 orders of magnitude the number of low-orbit sources of SHF electromagnetic radiation (EMR) in the direction of the earth's surface and also will increase in the total density of downlink satellite communication area traffic capacity on the earth's surface, especially when integrating these satellite communication systems with global 5G/6G mobile communication systems.

This alarms specialists who are concerned about both the obvious increase in the probability of collisions of satellites of various affiliations and the problem of “space debris” [1, 2], and the expected complication of the electromagnetic environment (EME) near the earth’s surface, which may cause interference for various terrestrial radio services that use frequency bands of satellite systems on a secondary basis, as well as aggravation of problems of electromagnetic safety of the population and electromagnetic ecology of the habitat [3, 4].

The goal of this work is to summarize a base technique and models presented in [5] that makes it possible to analyse EME presented as an ensemble of radio frequency electromagnetic fields (EMF) created near the earth's surface by EMRs of megaconstellations of low earth orbit satellites (LEOS).

2 Initial models and assumptions

A. Model of LEOS radiation to the earth's surface

The main LEOS megaconstellations are characterized by layered placement of subsets (separate constellations) of satellites in different orbital planes and with different orbital inclinations, ensuring their uniform quasi-regular distribution above the Earth's surface [5].

From a ground-based observation point (OP), the location of N satellites of the LEOS megaconstellation in n spherical orbital shells of radii $R_i = H_i + R_E$, $i \in [1, n]$ over N_i satellites in the shell can be considered random and uniform over the shell area with an average density ρ_i [LEOS/m^2]:

$$N = \sum_{i=1}^{n} N_i, \quad \rho_i = N_i \Big/ \left[4\pi\left(H_i + R_E\right)^2\right], \tag{1}$$

where 300 km ≤ H_i ≤ 2000 km is the altitude of the orbit of the i-th LEOS constellation, R_E is the Earth radius.

As a model of the LEOS antenna radiation pattern in the direction of the earth's surface, a two-level model with a conical beam of equal width $\Delta\varphi$ in azimuth α and zenith angle β can be used, described by the following relations:

$$\left.\begin{aligned} G_{ML} &= \frac{C_P}{\left(1+C_P\right)sin^2\left(\Delta\varphi/4\right)}, C_P = \frac{P_{ML}}{P_{SL}}, P_{ML}+P_{SL} = P_{TRP};\\ G_{SLR} &= \frac{G_{SL}}{G_{ML}} = \frac{tg^2\left(\Delta\varphi/4\right)}{C_P}; G_{SL} = \frac{1}{\left(1+C_P\right)cos^2\left(\Delta\varphi/4\right)};\\ g_N\left(\alpha,\beta\right) &= \begin{cases} 1, & \alpha,\beta \in \Delta\Omega_{ML};\\ G_{SLR} = tg^2\left(\Delta\varphi/4\right)\big/C_P, & \alpha,\beta \in \Delta\Omega_{SL}, \end{cases} \end{aligned}\right\} \tag{2}$$

where G_{ML} is the gain in the main lobe (ML), G_{SL} and G_{SLR} are absolute and relative levels of side lobes (SL), C_P is the ratios of powers emitted in the ML (P_{ML}) and SLs (P_{SL}), respectively; $\Delta\Omega_{ML}$ and $\Delta\Omega_{SL}$ – solid angles corresponding to the main and side lobes, $g_N(\alpha,\beta)$ – normalized radiation pattern, P_{TRP} – LEOS total radiated power.

Since all LEOS in a constellation can be considered the identical, their equivalent isotropically radiated powers (EIRP) both in ML ($P_{eML}=G_{ML}P_{TRP}$) and SL $P_{eSL}=G_{SL}P_{TRP}=G_{SLR}P_{eML}$) can also be considered the identical.

The potential LEOS service area is limited by the minimum elevation angles ε_{min} of arrival of signals at the terrestrial user equipment (UE) and the maximum length of the LEOS-to-UE radio link is equal to R_{max} (Fig. 1). The actual LEOS service area determined by an inclined ML position has the form of a spot, which is roughly close in shape to an ellipse with axes L_X, L_Y having area $S_S \approx \pi L_X L_Y$.

The curvature of the Earth surface and the LEOS orbital shells determines the difference between the minimum viewing angle of a LEOS from a ground-based OP and the minimum viewing angle of a given OP from that LEOS: $\varepsilon_{min} > \theta_{min}$ (Fig. 2).

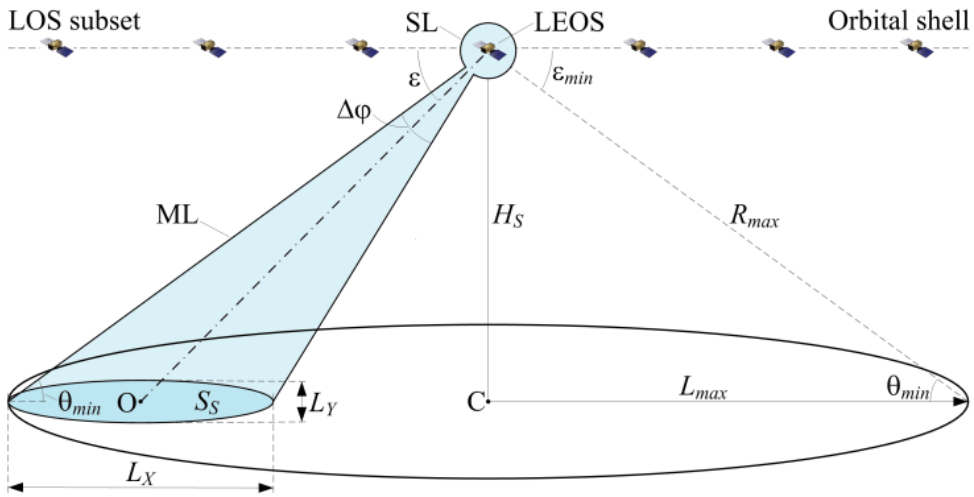

Fig. 1. Direction of the ML of LEOS EMR onto the earth's surface at $\varepsilon = \varepsilon_{min} + \Delta\varphi/2$; O – point of intersection of ML axis with earth's surface.

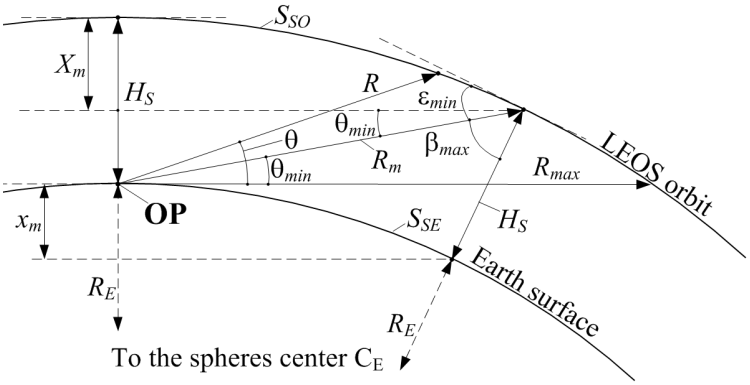

Fig. 2. Model of OP location on the earth's surface and of the part of LEOS canstellation in a spherical segment of height X_m and area S_{SO} of an orbital shell of height H_S, which provide irradiation of the earth's surface from viewing angles $\varepsilon \in [\varepsilon_{min}, 90^{\circ}]$.

The relationship between these angles is determined by the following relations:

$$\left.\begin{aligned} \varepsilon_{min} &= \frac{\pi}{2} - \beta_{max} = \frac{\pi}{2} - arccos\left(\frac{(H_S + R_E)^2 + R_m^2 - R_E^2}{2(H_S + R_E)R_m}\right); \\ R_m &= \sqrt{R_E^2 \sin^2\theta_{min} + H_S^2 + 2R_E H_S} - R_E \sin\theta_{min}, \end{aligned}\right\} \quad (3)$$

where R_m is the maximum distance between LEOS and OP at $90^o \geq \theta \geq \theta_{min}$, β_{max} is the maximum angle between the perpendicular to the earth's surface (nadir) at the LEOS location point and the direction to the border of its potential service area, determined by the value θ_{min}. Distance R_{max} in Figure 2 corresponds to the line-of-side distance of LEOS from OP at $\theta = 0$.

B. Model of RWP conditions

We will assume that all analysed OPs of the earth's surface are in direct visibility from the orbital positions of LEOS – EMR sources, which allows us to use the worst-case model of radio wave propagation conditions (RWP) in free space:

$$Z = P_e / \left(4\pi R^2\right), \tag{4}$$

where P_e is the LEOS EIRP, R is the distance between the OP and the LEOS; Z [W/m^2] is the scalar power flux density (PFD) of EMF created in OP by LEOS EMR.

C. Electromagnetic background (EMB) in OP, created by LEOS radiations

The intensity Z_Σ of EMB created in OP by the set M of LEOS – EMR sources is defined as the scalar sum of M random PFD values of radiofrequency EMFs reached the OP:

$$Z_\Sigma = \sum_{m=1}^{M} Z_m \, . \tag{5}$$

D. Algorithm for Analysing the EME Characteristics

The technique of system analysis of the EME characteristics near the earth's surface created by LEOS constellations is based on the results of [6, 7, 10, 11] and involves the sequential implementation of the following procedures:

a) Define the analyzed EMR scenario of the LEOS constellation in dependence on the corresponding characteristics of the mutual spatial location of the OP, randomly selected on the earth's surface, number N_{ML} of LEOSs, which irradiate OP by main lobe with EIRP P_{eML}, and number N_{SL} of LEOSs, which irradiate OP by side lobe with EIRP P_{eSL}.

b) Define the probability distribution densities (p.d.d.) $w_{ML}(R)$, $w_{SL}(R)$ of distances from LEOS irradiating the earth's surface by ML and SL with EIRP P_{eML} and P_{eSL} to the OP.

c) Define p.d.d. $w_{ML}(Z)$, $w_{SL}(Z)$ of PFDs created in OP by LEOSs radiation via ML and SL respectively, as p.d.d. of random variable transformed using the inversion of (4) with $P_e = P_{eML}$ or $P_e = P_{eSL}$:

$$w(Z) = w\left(R = \Phi^{-1}(Z)\right)\left|dR/dZ\right|, \quad R = \Phi^{-1}(Z) = \sqrt{P_e/(4\pi Z)} \, . \tag{6}$$

d) Determine the expectations $m_1(Z_{ML})$ and $m_1(Z_{SL})$ for PFDs created in OP by ML and SL of LEOS antennas.

e) Determine the average EMB components $Z_{\Sigma ML}$ and $Z_{\Sigma SL}$ created in OP by LEOS ML and SL respectively as the products of the average number of corresponding LEOS (N_{ML}, N_{SL}) determined at stage "*a*", and the average PFD values ($m_1(Z_{ML})$, $m_1(Z_{SL})$, see item "*d*"):

$$Z_{\Sigma ML} = N_{ML} \cdot m_1(Z_{ML}), \quad Z_{\Sigma SL} = N_{SL} \cdot m_1(Z_{SL}) \, . \tag{7}$$

f) Determination of the total average EMB level Z_Σ in OP as the sum of components formed by ML and SL radiations of the given set of LEOS:

$$Z_\Sigma = Z_{\Sigma ML} + Z_{\Sigma SL} \, . \tag{8}$$

3 Analysis of LEOS constellations spatial models and Earth irradiation scenarios

Since satellite systems may differ in EMR characteristics in the direction of the earth's surface, an analysis of EMR characteristics for several LEOS EMR implementation scenarios was performed using the above algorithm.

A. LEOS with isotropic EMR, scenario 1 (hypothetic)

A model of the spatial placement of the LEOS constellation with isotropic EMR and OP on the Earth's surface is shown in Figure 3.

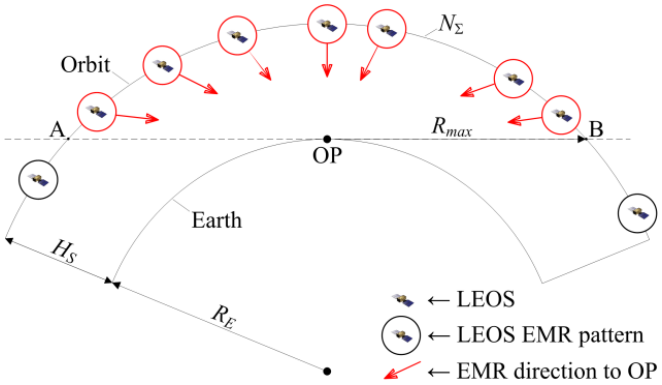

Fig. 3. Spherical model of the distributed above the earth's surface constellation of LEOS with isotropic EMR. LEOS from radio visibility zone capable of OP irradiating are highlighted in red.

If LEOS are distributed uniformly with density ρ_i = *const* over the *i*-th orbital shell of height H_S, then their average number in the shell segment limited by the radio visibility zone of radius R_{max} from OP is equal to

$$N_\Sigma = 2\pi\rho_i(R_E + H_S)H_S\,. \tag{9}$$

Using the algorithm described above, for the considered scenario we obtain the following:

a) P.d.d. $w(R)$ of the distance R from LEOS to the OP:

$$w(R) = R/(H_S R_E),\ H_S \le R \le R_{max} = \sqrt{2R_E H_S + H_S^2}\,. \tag{10}$$

b) P.d.d. of PFD Z created in OP by LEOS with EIRP P_e:

$$\left.\begin{aligned} w(Z) = Z_{min}Z_{max}/\left[(Z_{max} - Z_{min})Z^2\right],\ \ Z_{min} < Z < Z_{max}\,, \\ Z_{min} = P_e/(4\pi R_{max}^2),\ \ Z_{max} = P_e/(4\pi H_S^2) \end{aligned}\right\} \tag{11}$$

c) The expectation $m_1(Z)$ is determined by the relation

$$\left.\begin{aligned} m_1(Z) = \int_{Z_{min}}^{Z_{max}} Z\cdot w(Z)dZ = \frac{Z_{min}Z_{max}}{(Z_{max} - Z_{min})} ln\frac{Z_{max}}{Z_{min}} = \\ = P_e\, ln\left[(2R_E + H_S)/H_S\right]/(8\pi H_S R_E). \end{aligned}\right\} \tag{12}$$

d) The average value Z_Σ of the EMB in OP:

$$Z_\Sigma = N_\Sigma \cdot m_1(Z) = \frac{\rho_i P_e (R_E + H_S)}{4R_E} \ln\left[\frac{2R_E + H_S}{H_S}\right] \tag{13}$$

B. LEOS with cuasi-isotropic EMR, scenario 2

In Scenario 2 (Fig. 4) LEOS EMRs are isotropic only for OP on the earth's surface; radiations occurs only in the direction of the Earth in the solid angle $\Omega_E = 2\pi(1-cos\beta_{max})$, corresponding to $\theta_{min} = 0$ and to the following value of β_{max} :

$$\beta_{max} = arccos\left\{\left[(H_S + R_E)^2 + R_{max}^2 - R_E^2\right] / \left[2(H_S + R_E)R_{max}\right]\right\}. \tag{14}$$

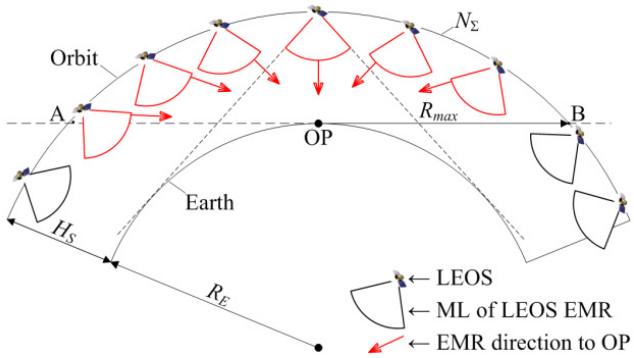

Fig. 4. Spherical model of the distributed above the earth's surface constellation of LEOS with quasi-isotropic EMR. LEOS from radio visibility zone capable of OP irradiating are highlighted in red.

In this case, at a fixed total radiated power P_{TRP} the LEOS EIRP in the direction of the earth's surface will increase relative the previous case (13) by an amount K_P equal to the ratio $4\pi/\Omega_E$, and the average EMB level at the earth's surface will be determined by the following ratio:

$$\left.\begin{aligned} Z_\Sigma &= \rho_i P_e K_P (R_E + H_S) ln\left[(2R_E + H_S)/H_S\right]/4R_E, \\ K_P &= 2(H_S + R_E)\Big/\left(H_S + R_E - \sqrt{H_S^2 + 2R_E H_S}\right), \\ \Omega_E &= 2\pi\left[1 - \sqrt{H_S^2 + 2R_E H_S}\,/(H_S + R_E)\right]. \end{aligned}\right\} \tag{15}$$

C. LEOS with vertical directional EMR, limited size of service area, scenario 3.

If the service area of LEOS with a relatively wide ML is limited by the elevation angle θ_{min} of its observation from the ground OP (Fig. 5), then the following occurs:

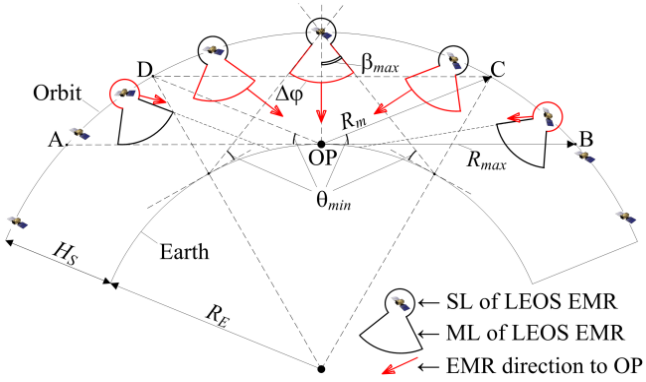

Fig. 5. Spherical model of the distributed above the earth's surface constellation of LEOS with wide conical ML and vertical EMR. Parts of LEOS EMR patterns capable of OP irradiating are highlighted in red.

a) LEOS EMRs are not isotropic; their antennas with a radiation pattern (2) are oriented vertically down to the nadir and provide service in the range of elevation angles $\theta \in [\theta_{min}, 90°]$. This is determined by the ML conical shape with width $\Delta\varphi$, equal to twice the value of the maximum viewing angle from OP: $\Delta\varphi = 2\beta_{max}$. The width $\Delta\varphi$ of the LEOS EMR ML turns out to be related to the value θ_{min} and the altitude H_S of the LEOS orbit, which determine the value of the maximum viewing angle β_{max} of OP at the orbital point observed from the OP under the angle θ_{min}.

b) EIRP of LEOS in ML (P_{eML}) and SL (P_{eSL}) are determined by the P_{TRP} value and the antenna gains (2).

c) Localization area on the orbital shell of the LEOS set irradiating the OP by MLs, is a spherical segment with height X_m (Fig. 2), determined by the R_m (3), and the base diameter DC in Fig. 5; p.d.d. of the distance R from these LEOS to the OP has the following form

$$w(R) = 2R/\left(R_m^2 - H_S^2\right),\ H_S \le R \le R_m\,. \tag{16}$$

d) Localization area on the orbital shell of the LEOS set irradiating the OP by SLs, is a spherical belt ABCD in Figure 5; p.d.d. of the distance R from these LEOS to the OP retains the form (16) for $R_m \le R \le R_{max}$.

For this scenario, expressions (7) for the average EMB intensity created in the OP by LEOS radiations along the main ($Z_{\Sigma ML}$) and side ($Z_{\Sigma SL}$) lobes, have the following forms:

$$Z_{\Sigma ML} = \frac{\rho P_{TRP} G_{ML} \left(R_E + H_S\right)\left(H_S - R_m \sin\theta_{min}\right)}{R_m^2 - H_S^2} ln\frac{R_m}{H_S};\tag{17}$$

$$Z_{\Sigma SL} = \frac{P_{TRP} G_{ML} \rho \left(R_E + H_S\right) R_m \sin\theta_{min} tg^2\frac{\Delta\varphi}{4}}{C_P\left(R_{max}^2 - R_m^2\right)} ln\frac{R_{max}}{R_m}\,.\tag{18}$$

D. LEOS with inclined narrow ML, scenario 4.

This scenario (Fig. 6) is most adequate to the analysis of Starlink LEOS constellations, the ML width $\Delta\varphi$ in which is 3.5º–5.5º depending on the angle of beam inclination, and many orbit inclinations for many orbital planes allows to consider the ML azimuth of a separate LEOS in the radio visibility zone from OP equal to the random equiprobable with its relatively small constant elevation angle θ_{min} (Fig. 1) which provides the required service zone for the ground-based UE in the LEOS moving direction.

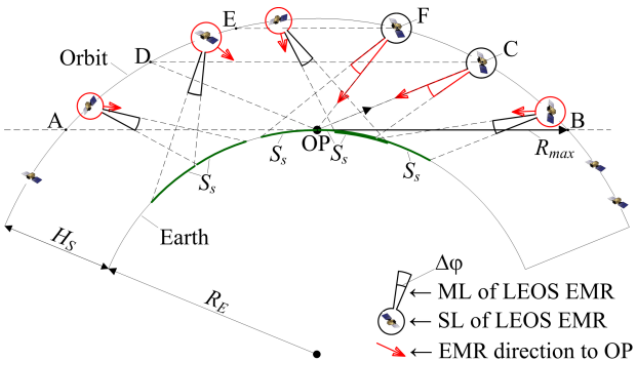

Fig. 6. Model of the distributed above the earth's surface constellation of LEOS with narrow conical ML inclined in different directions. Parts of LEOS EMR patterns capable of OP irradiating are highlighted in red.

Due to the noted differences of this scenario from the previously considered, at its analysis a different approach was used, based on scalar averaging the set of EMFs PFD radiated by LEOS, along the earth's surface, as well as a probabilistic approach based on the representation of the irradiation of the ground OP by LEOS ML as a rare event and determining the average EMB level in OP using Poisson probabilistic model.

Area S_S of the "spot" on the earth's surface (Fig. 1), irradiated by the LEOS narrow conical beam with a width of $\Delta\varphi$, is determined by the following expressions:

$$\left.\begin{array}{c} S_S \approx \pi \cdot L_X L_Y / 4; \quad L_Y \approx 2H_S tg(\Delta\varphi/2) / sin(\varepsilon); \\ L_X = H_S \cdot \dfrac{tg(\varepsilon + 0.5\Delta\varphi) - tg(\varepsilon - 0.5\Delta\varphi)}{tg(\varepsilon + 0.5\Delta\varphi) tg(\varepsilon - 0.5\Delta\varphi)}. \end{array}\right\} \quad (19)$$

The relative total average area S_{RA} of irradiation of the earth's surface by the constellation of N_Σ LEOS in the orbital shell with orbit height H_S, will be equal to:

$$S_{RA} = N_\Sigma S_S / S_E \approx \pi L_X L_Y N_\Sigma / (4 S_E), \quad S_E = 4\pi R_E^2. \quad (20)$$

Estimates using (18), allow us to conclude that upon completion of the Starlink system ($N_\Sigma \approx 30\,000$ on 10-15 orbital shells with altitudes ranging from 340 to 640 km), a scenario assuming an inclined position of the ML with an elevation angle $\theta_{min} = 25°$, provides almost complete “single-layer” coverage of the entire earth’s surface, in which any point on the surface at any given time is in the service area of at least one of the LEOS.

Since the S_{RA} parameter can be interpreted as the average number of LEOS MLs irradiating an OP at an arbitrary moment, we can assume that the probability $p(k)$ of its irradiation at that moment by a specific number k of LEOS is determined by the Poisson distribution:

$$p(k) = S_{RA}^k exp(- S_{RA}) / k!. \quad (21)$$

The average PFD Z_a created in the “spot” of LEOS ML on the earth’s surface is equal to:

$$Z_a \approx \left(C_P P_{TRP} \sin^2 \varepsilon\right) / \left[4\pi H_S^2 (1 + C_P) \sin^2 (\Delta\varphi/4)\right]. \quad (22)$$

At the discrete distribution (21) of the probabilities of an OP falling into the service area of exactly k LEOS MLs, the average EMB intensity created in this OP is equal to:

$$Z_{\Sigma ML} = \sum_{k=1}^{K_m} k Z_a p(k), \quad K_m >> 1. \quad (23)$$

It is obvious that the adequacy of Poisson model in relation to the considered scenario is limited, since the relative OP and LEOS position cannot be considered completely random, since the relative position of LEOS in the orbital shell of constellation has the regularity necessary to ensure acceptable waiting times and a minimum probability of UE service failure. But taking into account the presence of many orbital shells in constellation, as well as the independence of separate LEOS constellations and relative smallness of S_{RA}, positions of LEOS relative to OP can be considered random, and model (23) can be considered adequate under certain restrictions on k values.

The number $N_{\Sigma SL}$ of LEOS irradiating the earth's surface by SLs is determined by the number N_Σ of LEOS in the radio visibility zone from OP and the ratio of the solid angle Ω_{ML}, corresponding to ML, and the solid angle Ω_H, subtended by the earth's surface along the horizon and corresponding to the angle β_{max} (14) at $\theta_{min} = 0$:

$$\left.\begin{array}{c} N_{\Sigma SL} = N_\Sigma (\Omega_H - \Omega_{ML}) / \Omega_H \\ \Omega_H = 2\pi\left(1 - \sqrt{H_S^2 + 2R_E H_S} / (H_S + R_E)\right) \\ \Omega_{ML} = 2\pi(1 - cos(\Delta\varphi/2)) \end{array}\right\}; \quad (24)$$

LEOS SL radiations in the direction of the earth's surface are considered isotropic in a solid angle of magnitude $\Omega_H - \Omega_{ML}$, therefore, to determine the average EMB intensity $Z_{\Sigma SL}$ created by these radiations at the earth's surface, we can use relations (12, 13) for isotropic LEOS EMR (scenario 1) by substituting into them P_{eSL} of SL EIRP values:

$$\left.\begin{aligned} P_{eSL} &= P_{TRP} \Big/ \left((1 + C_P)\cos^2(\Delta\varphi/4)\right), \\ Z_{\Sigma SL} &= N_{\Sigma SL} P_{eSL} \ln(R_{max}/H_S) \Big/ \left[2\pi\left(R_{max}^2 - H_S^2\right)\right], \end{aligned}\right\} \quad (25)$$

the average total EMB level Z_{Σ} is determined similarly to (8) as the sum of (23) and (25).

4 Quantitative analysis of average EMB intensity at the considered scenarios

Analysis of dependences of EMB components $Z_{\Sigma ML}$, $Z_{\Sigma SL}$ and of the total level Z_{Σ} of the average EMB intensity created by LEOS ML EMRs at the earth's surface for different scenarios on the quantity N_{Σ} of LEOS in the constellation with typical parameters $P_{TRP} = 100$ W, $H_S = 550$ km, indicates the following:

1) EMB level at the earth's surface significantly depends on the C_P parameter, which characterizes the loss of EMR power due to the SLs, which reduces the part of the LEOS total radiated power P_{TRP} that reaches the earth's surface. At an increase in C_P and a decrease in θ_{min}, the dependences $Z_{\Sigma}(N_{\Sigma})$ tend to the pessimistic one peculiar to scenario 2 (relation (15)), in which all energy radiated by LEOS falls on the earth's surface. In scenarios 3, 4, with a fixed P_{TRP} and excluding MLs from falling beyond the earth's surface ($\theta_{min} - \Delta\varphi/2 > 0$), a change in ML width is accompanied by a corresponding change in G_{ML} and ML EIRP with practical constancy of the covering total radiated power – the P_{TRP} fraction, emitted in solid angle Ω_H (24) [7]. Therefore, for given N_{Σ}, θ_{min}, P_{TRP} and C_P, the average EMB intensity at the Earth's surface is practically independent of ML width $\Delta\varphi$ and on LEOS orbit height H_S. At multi-beam LEOS EMR, an increase in the number of beams is accompanied by a decrease in the radiated power of each beam in such a way that the total radiated power P_{TRP} remains constant, limited by LEOS energy capabilities, which can be interpreted as an expansion of the equivalent single ML, under the accepted restrictions does not affecting on the average intensity of the created EMB.

2) The very weak dependence of the average EMB intensity created by the LEOS constellation at the earth's surface on the orbital altitude H_S, noted above in relation to scenarios 3, 4, indicates the applicability of (17-25), at least for analyzing the EMB intensity created by the entire constellation of non-geostationary satellite communication and navigation systems, in particular, global navigation satellite systems GPS, GLONASS, Galileo, Beidou, etc.

3) Pessimistic estimates of the average EMB levels created by LEOS constellations (worst case estimates) can be performed using relation (15), and a more detailed analysis using (17-19, 23, 25) allows to assess the impact on the average EMB levels of the power efficiency and directionality of LEOS EMR (parameters C_P, $\Delta\varphi$), orbit altitudes H_S, restrictions on the elevation angle θ_{min} of the served LEOS, etc.

5 Conclusion

The above relations (9-19, 23, 25), obtained as a result of the analysis of several operation scenarios for the LEOS constellations, provide the possibility of a preliminary multivariant pessimistic (worst-case) quantitative analysis of the average intensity of the EMB created by these systems near the earth's surface. The results obtained using probabilistic schemes (6) and (21-23) are practically identical, which in general can be

considered as evidence of the adequacy of these different approaches and methods for analyzing the average EMB intensity created by LEOS constellations.

Comparison of the average level of natural EMB in SHF frequency band, which is of about $10^{-20}…10^{-19}$ W/m^2 according to [8], with the average levels of artificial EMB created by the LEOS megaconstellations indicates that these levels can exceed the level of natural EMB by many orders of magnitude. And although, in general, levels of artificial EMB created by the radiation of LEOS megaconstellations remain quite low, such a quantitatively significant change in physical characteristics of the operating environment of ground-based technical systems and the habitat of the population requires serious attention and analysis.

Taking into account the problem relevance, presented results require further development and clarification. In terms of a more detailed comparison of the EMB levels created by LEOS megaconstellation emissions with various components of natural EMB created by extraterrestrial sources. In accordance with [9], as well as the EMB levels created by the subscriber terminals emissions of satellite communication systems.

REFERENCES

[1] [S.S. Veniaminov, A.M. Chervonov, “Space Debris – a Threat to Mankind,” Moscow, IKI, 2012, 191 p. (in Russ.)

[2] “Risk Associated with Reentry Disposal of Satellites from Proposed Large Constellations in Low Earth Orbit,” *FAA Report to Congress*, Sept. 22, 2023.

[3] O.A. Grigoriev and Y.B. Zubarev, “The effects of wireless communication electromagnetic energy influence on persons: predictions of the growth for conditioned morbidity, their implementation and problems of evaluation,” *CONCEPCII*, No.1 (41), 2022, pp. 3-17. DOI: 10.34705/KO.2022.68.54.001

[4] J. Martel, “Did low Earth orbit internet satellites trigger the COVID-19 pandemic?”, *NEXUS*. Vol. 30, No. 3, 2023, pp. 35-43, 82-83.

[5] V. Mordachev, D. Tsyanenka, A.Svistunou, “Characteristics of Electromagnetic Environment Created by Communication Low Earth Orbit Satellite Systems Near the Earth's Surface,” *Proc. of the Int. Symp. “EMC Europe 2024”*, Bruges, Belgium, Sept. 2–5, 2024, pp. 1178-1183.

[6] V. Mordachev, “System ecology of cellular communications,” Minsk, BSU Publishers, 2009, 319 p.

[7] V. Mordachev, “Electromagnetic Background Generated by Mobile (Cellular) Communications,” *Proc. of “APEMC-2021”*, Bali-Indonesia, Sept. 27-30, 2021, pp. 37-40.

[8] P. Bandara, D.O. Carpenter, “Planetary electromagnetic pollution: it is time to assess its impact,” *The Lancet Planetary Health*. Vol.2, Dec. 2018, e512–e514. DOI:10.1016/s2542-5196(18)30221-3.

[9] Recommendation ITU-R P.372-16 – Radio noise (08/2022).

[10] A. Pastukh, V. Tikhvinskiy, S. Dymkova, O. Varlamov "Challenges of Using the L-Band and S-Band for Direct-to-Cellular Satellite 5G-6G NTN Systems," *Technologies*, 2023, 11(4), 110. doi:10.3390/technologies11040110.

[11] A.S. Pastukh, V.O. Tikhvinskiy, E.E. Devyatkin, A.A. Savochkin, A.V. Lukyanchikov "Electromagnetic compatibility studies between HAPS and IMT terrestrial networks of legacy mobile standards (GSM, UMTS, LTE) in the frequency bands below 2.7 GHz," *T-Comm*, 2024, vol. 18, no.5, pp. 49-60. doi: 10.36724/2072-8735-2024-18-5-49-60.

SYNCHROINFO JOURNAL

www.media-publisher.eu/synchroinfo-journal

VOICE OVER IP TO ISDN GATEWAY VIA LTE ACCESS

Valeriy V. Polyanov[1], **Sergey V. Toropov**[2]

[1] Siberian Transport University, senior lecturer, Novosibirsk, Russia;

polyanovvv@mail.ru

[2] OJSC Russian Railways, Head of division of the Novosibirsk regional communications center, Novosibirsk, Russia;

toropovs@wsr.ru

ABSTRACT

The relevance of article is due to the developing and increasing of telecommunication network kinds and access technologies in railway infrastructure including Long-Term Evolution (LTE). An important practice task is to realize interaction between both developing and existing networks such as Voice over Internet Protocol (VoIP), Integrated Services Digital Network (ISDN), etc. The object of the study is access gateway to the railway operation network via LTE access for fixed and mobile subscribers. This solution might provide access to existing ISDN for a distance more than 1 km without signal regeneration and installation of additional expensive equipment, redundant in the case of access by a small number of subscribers. Thus, this study is aimed at hardware and software based solutions of the VoIP to ISDN gateway via LTE construction system. The paper proposes test of the gateway operation, as well as experiments using IP and ISDN protocol analyzers to describe the interaction of network signaling, estimated the sizes of data transmission packets for several types of codecs. Authors note that further research of the device should be carried out using the QoS criteria depending on the operating conditions of the LTE network (signal level, object speed, presence of obstacles and signal reflections).

DOI: 10.36724/2664-066X-2024-10-4-31-42

Received: 24.06.2024
Accepted: 15.07.2024

Citation: V.V. Polyanov, S.V. Toropov, "Voice over IP to ISDN gateway via LTE access" *Synchroinfo Journal* **2024**, vol. 10, no. 4, pp. 31-42

KEYWORDS: *Long-Term Evolution, LTE, ISDN, railway telecommunication, Voice over Internet Protocol, gateway*

1 Introduction

Advanced technologies and developing of a common information space on railway transport allow making operational communication in a universal tool. VoIP technology plays an important role in telecommunication infrastructure of NGN (New Generation Networks) because it solves the problems of voice, video and data transmission. Quality of services (QoS) provided by VoIP networks becomes better every year thanks to the new types of signaling and speech coding algorithms. Currently, VoIP has a wide variety of services, integrated monitoring and management tools [1].

Because of the implementation of packet switching technology, many companies replace existing analogue equipment and digital PBX for IP one. Railway divisions also implement it as a tool of transportation management. Number of VoIP subscribers on railway infrastructure increase rapidly due to call quality and wide range of services. However, the most of services for transportation processes are still based on ISDN and analogue channels because of existing large-scale infrastructure across the railway, interaction with remote control equipment on physical layer and high structure reliability. Taking into account a transportation operation usually occurs for dispatching division or railway station selectively. To make it work, existing ISDN and analogue networks should be able to interact with the network being implemented.

Gateways are usually used to communicate with PSTN (Public Switched Telephone Network) and VoIP-networks using different signaling protocols and protocols for transmission of media flow, including VoIP networks, which are based on either open source (YATE) or proprietary (3CX) protocols [2,3].

VoIP to analogue PBX gateway solution is possible to realize via addition of ITG (Internet Telephony Gateway). Current researches discussed the analysis of voice quality in the communication process between telephone sets via ITG in a VoIP network based on the shape of the input and output, the amplitude response to frequency changes, information security, quality of service and delay [4,5]. Each terminal establishes connection to the classical time division multiplexing (TDM) via packet switching network. Terminals with packet switching are apart in the IP-network via a local area network. An important feature of VoIP is separation of connection and disconnection processions from the voice-packet transmission process. As a traditional TDM technology, VoIP communication is divided into three phases: establishment of connection, transferring of voice and disconnection. Signaling system is used to establish connection and disconnection. Furthermore, signaling system allows subscribers to use audio-, video- conferences and additional services. Signaling data provides administration system for traffic accounting, definition of services quality, calls billing and other purposes [6]. Currently, interaction already existing networks and developing ones is an important task for telecommunication infrastructure of railway transport.

One of technologies being adopted for railway systems is LTE, which implementing on railway areas in transportation processes. LTE based high-speed railway telecommunication network is more effective and reliable than GSM-R or analogue one [7]. The fast development of high-speed railway, as a high-mobility intelligent transportation system, and the growing demand of broadband services for users, introduce new challenges to wireless communication systems [8].

According to [9,10] future railways may reduce their operational costs and augment the traffic capacity by implementation, for example, Industrial Internet-of-Things (IoT) is based on developed wireless network, such as LTE. These measures are expected to improve the performance of key management systems, such as those related to traffic scheduling and transportation system capacity planning, along with railway transportation safety and energy efficiency, interoperability, and support to multimodal transportation. These systems can be integrated with the railway traffic control system. For example, European Rail Traffic Management System (ERTMS) is based on the technical specification for interoperability for "traffic-control and signal-safety" subsystems were designed by the European Union Railways Agency (ERA). IoT integration for train inspection in railway infrastructure, track monitoring and voice communication via LTE are described in [11].

It also necessary to study other possibilities of wireless telecommunications not only for railway cases, but also for public ones in open networks. One of them is an implementation LTE network for passenger comfort. It also possible to use an open system in the LTE for the transmission of signals for railway traffic control and passengers while maintaining an appropriate level of safety [12].

The International Union of Railways (UIC) is developing the Future Rail Mobile Communications System (FRMCS). The paper [13] describes the Adaptive Communications System (ACS), which is currently being developed jointly by the industry and a number of railway operators to cover all types of railway wireless networks, radio access technologies and transport infrastructure features. ACS could pave the way for innovation in the railway sector in the context of geographical and technological differences between railways in different countries and regions. LTE can be considered as a public network or a type of radio communication for train control. Article [14] describes the possibility of integrating these networks, analyzes the compatibility of their functions, and compares the requirements for developing public safety technology in LTE-R.

To organize interaction between PSTN segments and GSM wireless networks, research was carried of implementing a VoIP system using an integrated IP PBX server with telecommunication service providers. GSM VoIP gateway connection is described at article [15]. IP PBX system connected to a GSM network using a GSM VoIP gateway is designed and implemented. Another research [16] is aimed to evaluate the performance of GSM VoIP Gateway in the IP PBX system using quality of service (QoS). The SIPdroid softphone was selected as a subscriber device. The connection between the VoIP client and the GSM VoIP Gateway is classified as a good quality service, since it has an average jitter value of ≤ 5.7 ms, packet loss ≤ 0.18% and delay ≤ 9.41 ms.

Wireless data on railway infrastructure has prospects not only at train dispatching and signaling, but also it may provide access to ISDN or analog workplaces on railway stations. Already existing solutions for VoIP/LTE to ISDN gateway are based on core-PBX. The disadvantages of such solutions are excess capacity and high cost in case of installation at stations along the railway. Furthermore interaction between equipment of different vendors is not allowed or requires high costs generally. In case of organizing wireless access to a workplace within a station via LTE, distributed gateways with a small port capacity are required. Nevertheless, currently there is a problem in integrating LTE-R and existing railway telecommunication services from the perspective of functionality. That is why an actual task is to implement LTE as access network to existing ISDN.

At present, IP-based telephony networks in railway infrastructure use SIP as the main type of signaling. The signaling systems also include gateway's protocols such as MGCP (Media Getaway Control Protocol), MEGACO/H.248, SGCP (Simple Gateway Control Protocol), SIGTRAN (Signaling Transport – Protocol stack for provision reliable datagram services and user layer adaptations for Signaling System 7 (SS7) and ISDN communications protocols), STCP (Stream Control Transmission Protocol – Protocol of reliable delivery of packets in the IP-based networks), SCCP (Skinny Client Control Protocol – Corporative terminal protocol), Unistim (Private communication signaling protocol), IAX2 (Inter Asterisk eXchange protocol, v2) and others [17, 18].

The main object of the article is hardware and software solutions of VoIP-to-ISDN gateway in LTE access conditions. An important task is not only theoretical research of gateway, but also practical investigation of equipment and software used in packet-switched networks and mixed networks in order to implement it into railway telecommunication infrastructure. Since the article describes configuration of the required hard- and software of gateway solution; integration of the test system into the experimental environment; test of predefined communication scenarios including protocol analysis; traffic evaluation.

2 VoIP-to-ISDN via LTE laboratory setup

VoIP-to-ISDN via LTE gateway setup is based on IP-PBX software Asterisk. IP-PBX allows making calls using equipment that support standard SIP RFC 3261. Software implementation allows configuring all nodes of virtual PBX. It is possible to change requirements without designing or production a new equipment. Hardware requirements depend on capacity of the PBX, interaction with other PBX's or PSTN and set of additional services.

Asterisk operates as SIP-registrar and SIP proxy in VoIP-networks and also provides services of VoIP. Asterisk allows creating 5th class softswitches which are intended for work with end-users. This equipment is used for both local and long distance telephony services. Softswitches are characterized by additional services for end-users and corpo-

rate clients such as IP PBX features, call center services etc. This IP-PBX provides services for conference, group calling, voice-menu, forwarding of calls etc. [19]. It includes DNS-server, NTP-server and DHCP-server. Also, it is able to work as a platform for a gateway using additional hardware such as ISDN-card.

ISDN card HFC-2BDS0 is installed into IP-PBX in order to connect IP-PBX to ISDN one. This card has PCI interface to install at IP-PBX and BRI interface (point S/T) to interact with ISDN. S/T interface is defined by Recommendation I.430 ITU-T, the most important aspects of S/T are:

– use fo r conductors;
– the maxi um allowable distance is 1 km;
– su port configuration “point-to-point” or “point-to-multipoint”;
– data tra sfer rate is 192 kbit/s.

Figure 1 provides appearance of ISDN card which can work as an ISDN card for PC through PCI-interface. It may be used as terminal adapter, network terminal, PBX or ISDN-modem [20].

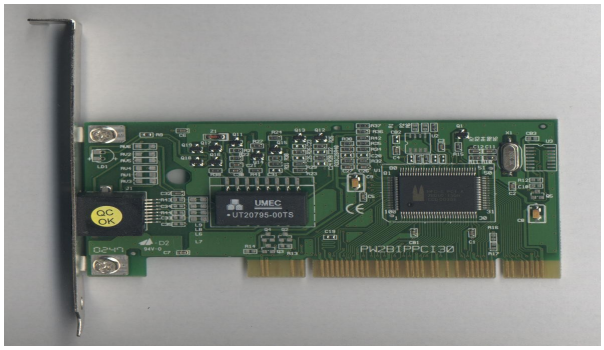

Fig. 1. ISDN card HFC-2BDS0

All necessary software (drivers) for correct work of ISDN card has been installed to IP-PBX. In this circuit, the card operates as the Network Termination of the first level – NT1 in "point-to-multipoint" mode. This mode is used to match electrical parameters of the line, control line status and conversion.

ISDN-side of complex includes ISDN-PBX with capability of 24 digital subscribers and 8 analogue subscribers. Protocol analyzer is connected to ISDN-network in order to decrypt messages of DSS-1. This device is also able to decrypt messages of 1TR6, Q-SIG, VN4, V 5.1, V 5.2, NI-1, and SS#7 [21]. ISDN analyzer could be placed between ISDN-card and ISDN PBX as well as between ISDN PBX and ISDN-phone. Figure 2 provides a schema of VoIP-to-ISDN gateway with equipment of ISDN-side and equipment for measurements in ISDN-side.

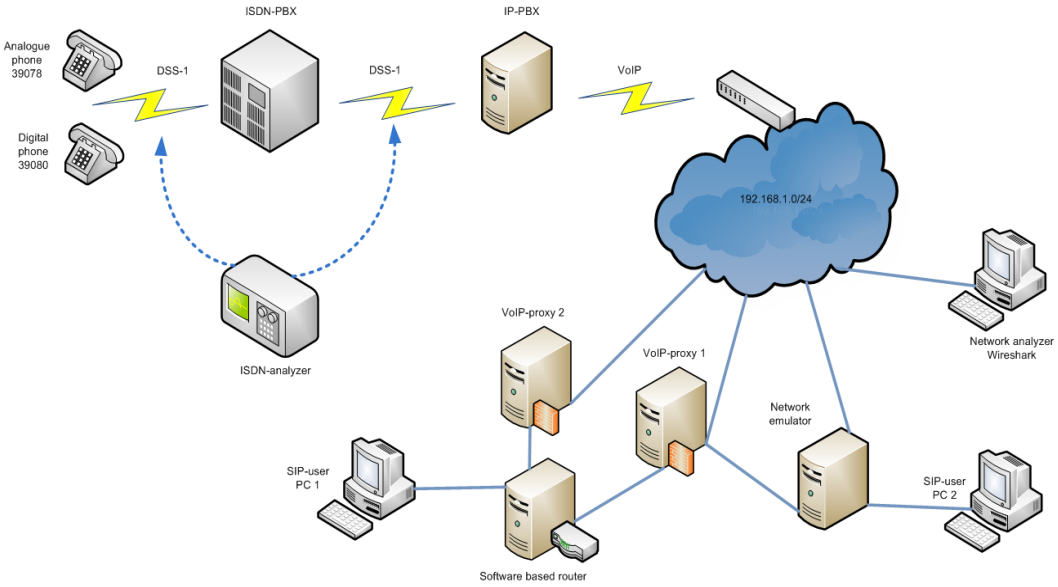

Fig. 2. Schema of VoIP-to-ISDN via LTE gateway

Network analyzer Wireshark has been also installed in the configuration. It allows capturing of IP-packets from Ethernet interface at local area network masked as /24. To achieve it all devices of this network are united by physical layer 8-port hub.

SIP-side of complex consists of two VoIP-proxies, software based router, software based network emulator and two SIP-subscribers. VoIP-proxies are based on software OpenSIP, which allows creating 4th class softswitch on PC. These softswitches are used for transit VoIP traffic between carriers. The main function of 4th class softswitch is the routing of large volumes of long distance VoIP calls. The most important characteristics are protocol support and conversion, transcoding, calls per second rate, average time of one call routing, number of concurrent calls. Software based router is used to create network layer static routes between different networks. Network emulator is used to delay and to make loss of the packets, which are flowed through emulator.

Softphones installed on PC1 and PC2 as sip-users. IP-PBX had been connected to network emulator via 8-port dual speed hub. Network-layer connection between IP-PBX-network and other networks were established by adding to main routing table on network emulator by utility “ip route add”.

IP-PBX should be registered on the proxy-voip2 as a subscriber to establish interaction with VoIP-proxies. For this purpose, is necessary to create new accounts in proxy-voip2 and define this proxy as SIP-provider for IP-PBX.

All accounts are located in the path of IP PBX server: *home/voipprak/Opensips/DB/subscriber. Accounts “1001”, “1002”*, and *“1150”* have been added to this file. Parameters of SIP-provider were determined in IP PBX.

Next step is to correspond external accounts of SIP-provider (proxy2) with internal extensions of IP-PBX (“Asterisk”). Thereby if any SIP-user from proxy2 (as well as from proxy1) calls to one of accounts “1001@voip2”, “1002@voip2” or “1150@voip2” this call will come to IP-PBX and then IP-PBX will forward this call to internal extension. But it is not possible to dial name of SIP-account from ISDN- or analog phone, because SIP- account contains letters. In order to provide calls from IP-PBX to proxy2 and proxy1 file: *etc/asterisk/extensions.conf* of IP-PBX server has been changed. This file contains dial plan configuration and defines processing and routing of incoming and outgoing calls. New scenarios of dial plan were added to make outgoing calls from IP PBX. Each extension has format shown below:

exten=>telephone number, priority, command

In this case new dial plans have been created for outgoing calls for *user1@voip2 and user2@voip1 by using command Dial()*, which can have one of two following formats:

Dial(type/identifier, timeout, options, URL)
Dial(type1/identifier1&type2/identifier2&type3/identifier3...,timeout, options, URL)

The command is trying to call on all specified channels simultaneously by type and identifier. As soon as one of the channels responds to a call for all other call is terminated. The first dial plan is shown below:

exten=>2001,1,Dial(SIP/user1@192.170.56.5)

It means, if any subscriber of IP-PBX (including ISDN-side) calls to „2001”, IP-PBX will dial subscriber user1@192.170.56.5 by channel known as SIP.

The second dial plan is used for outgoing calls to user2@192.170.34.3:

exten=>2002,1,Dial(SIP/user2@192.170.34.3,20,m)
exten=>2002,2,Dial(SIP/psgw@192.168.1.10)

This dial plan provides call to user2@192.170.34.3 for 20 seconds with music in background. If SIP-user user2@voip1 will not answer for this call during 20 seconds, IP-PBX will look at second priority of this dial plan and will call to SIP-user psgw@192.168.1.10.

Thereby, complex of gateways was successfully integrated into already existing environment of VoIP. It allows creating new scenarios for railway communication infrastructure.

3 Signaling analyzing

Analyzing of VoIP to ISDN via LTE connection signaling is based on corresponding messages between ISDN and VoIP network. In order to get DSS-1 data ISDN-analyzer is placed between IP-PBX and ISDN one. Network analyzer Wireshark is run across path of SIP-signaling via proxies to gateway. Connection between ISDN-phone and SIP-user is established to record DSS-1 data from ISDN-analyzer and SIP-messages from Wireshark. At first ISDN-analyzer is placed between ISDN-PBX and ISDN-phone, then it is replaced to ISDN-PBX gateway circuit. Picture 3 provides a schema of laboratory environment and an example screenshots of data from analyzers.

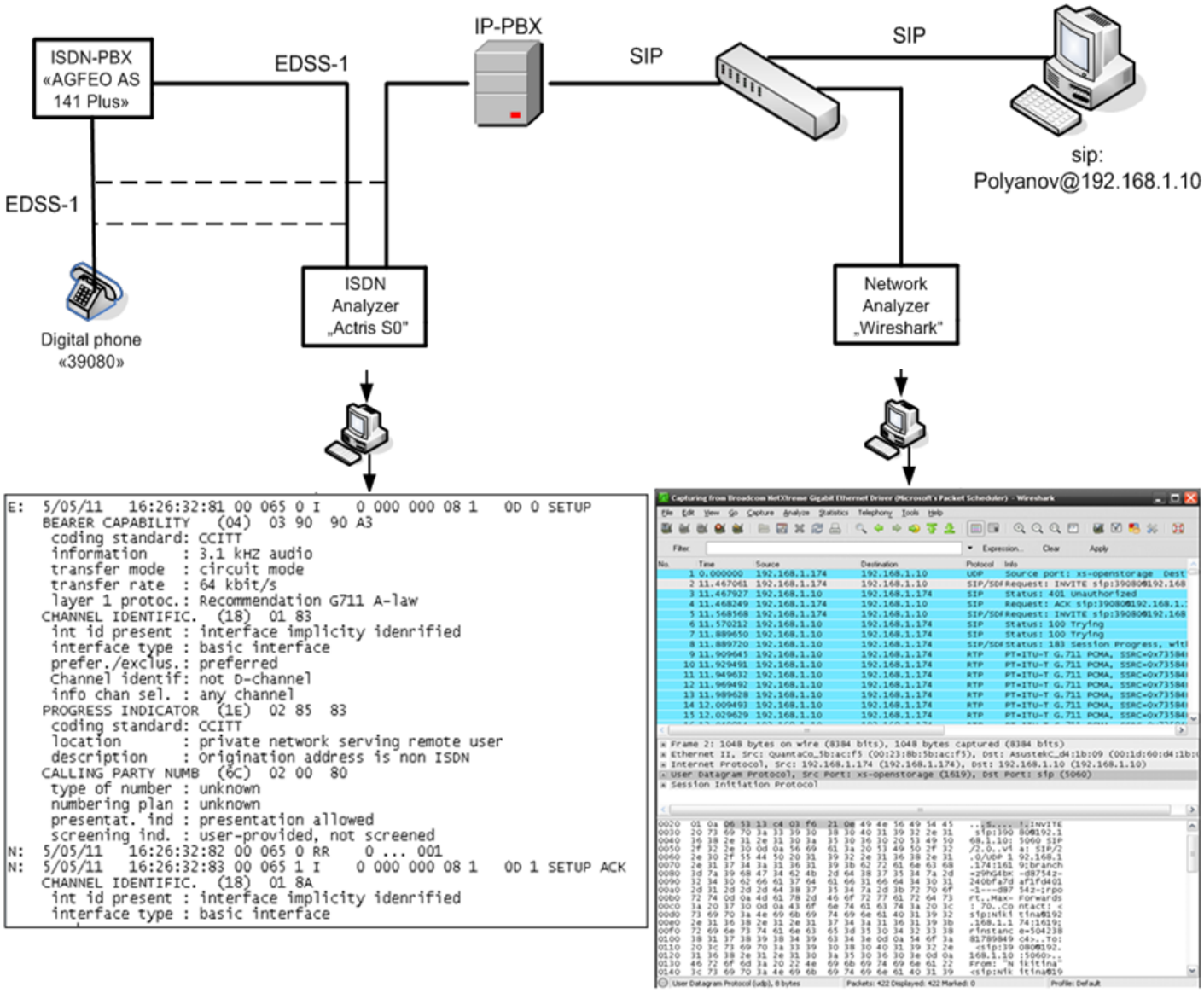

Fig. 3. Laboratory environment of signaling analysis

Figure 4 provides a graph of signaling processes between SIP-user and ISDN-subscriber. Data messages of second and third layers from ISDN analyzer were used to construct DSS-1 side of the graph. SIP-side of the graph is based on “Flow graph” function Wireshark application.

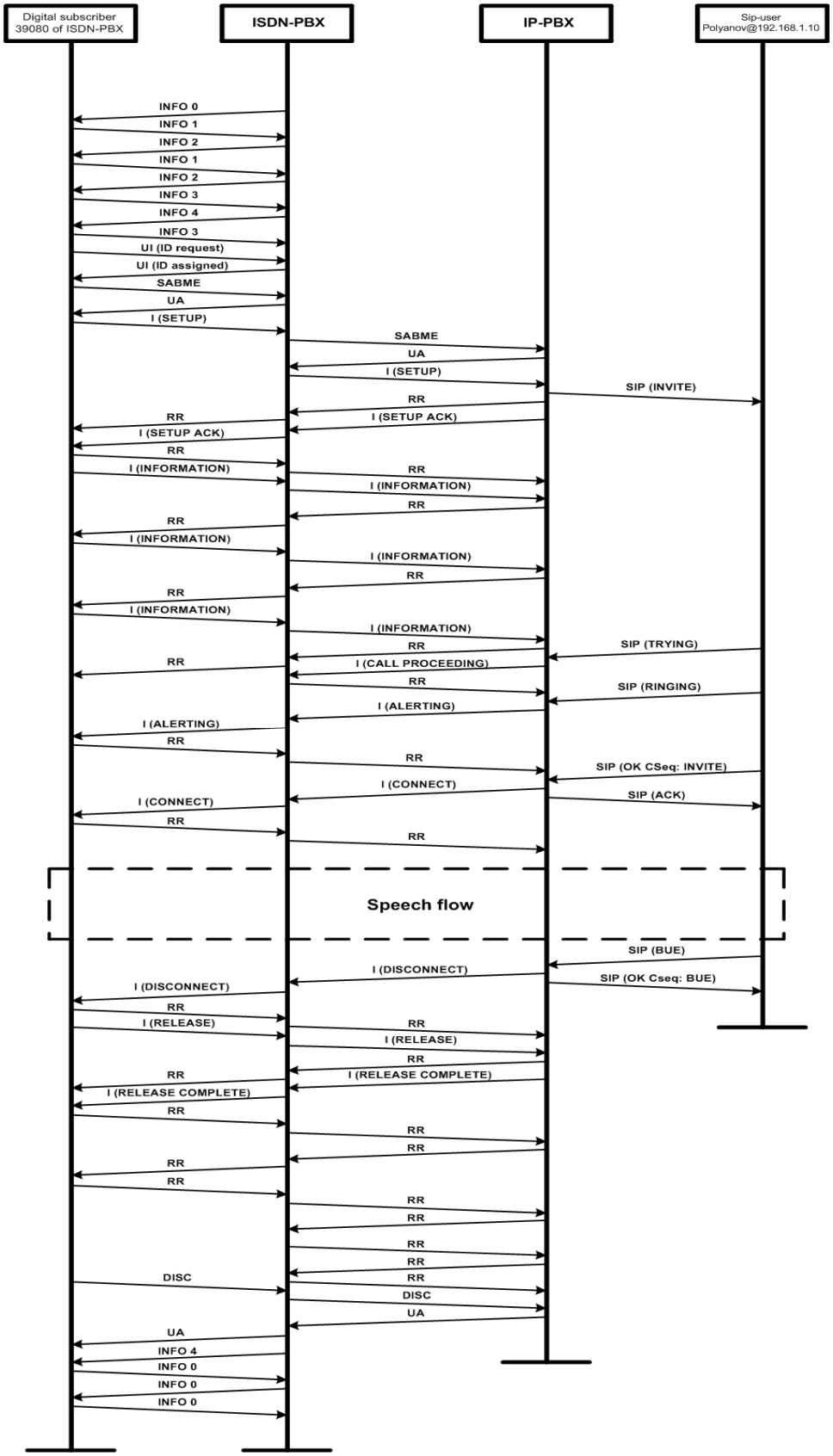

Fig. 4. Graph of signalling processes between SIP-user and ISDN-subscriber

The caller is ISDN-subscriber with extension “39080” and the callee is SIP-user Polyanov@192.168.1.10. Session between ISDN-phone and the PBX was started when subscriber “39080” pick headset up. Session connection to ISDN-network begins with conflict resolution access to the terminal. For this purpose ISDN-phone and PBX exchange INFO-messages (INFO0, INFO1, INFO2, INFO3, and INFO4). Each session ends by exchanging of INFO-messages.

The Terminal Equipment (TE) sends a request “IDrequest” to identify itself and then TE receives an answer with the ID of the terminal - TEI by unnumbered message. Before establishment of LAPD-connection (Link Access Procedure for D-channel), only unnumbered frames may be used for data-transmission. This process involves the transfer of command to Set Asynchronous Balanced Mode Extended (SABME). The recipient must respond by sending Unnumbered Acknowledgment (UA). Command DISC is used for LAPD. Second layer of DSS-1 can carriers messages of third layer after establishing of LAPD.

There two types of messages are defined in LAPD as reliable information (“I”) and unnumbered information (“UI”). Acknowledgments messages of type “I” are Receiver Ready “RR”.

Protocol Q.931 is used at the third level of DSS-1 to define the meaning and content of the signaling messages, in logical sequence of events and in the process of existence and the terminations of connections. Messages of the third layer of DSS-1 are transmitted by “I” - messages of LAPD. Some messages of the third layer of DSS-1 are corresponded with SIP-requests and SIP-answers in Table 1.

Table 1

Comparison of SIP- and DSS-1 messages purposes

Message of DSS-1	**SIP-request (answer)**	**Purpose**
SETUP	INVITE	Request to establish connection
SETUP ACK	OK CSeq: INVITE	Confirmation of request’s delivery
CALL PROCEEDING	TRYING	Extended search proceeding
ALERTING	RINGING	Sending ring-signal to subscriber
CONNECT	OK CSeq: INVITE	Subscriber answering
CONNECT ACK	ACK	Confirmation of answer’s request
DISCONNECT	BUE	Clear’s request
REALISE		Disconnection
REALISE COMPLETE	OK CSeq: BUE	Disconnection, clearing of resources

4 Estimation of minimum RTP-packet length

In order to implement the LTE network to ISDN access, the Round-Trip-Time (RTT) and downlink rate (DLR) parameters were estimated depending on the radio coverage level within four Base Transceiver Stations (BTS) in total at one railway station. Figure 5 shows results of RTT and DLR measurements. It was found that the RTT parameter is stable and varies within 40-60 ms when the radio signal level from the BS ranges from -70 to -120 dBm. There is no explicit correlation between the DLR and the coverage. However, at a critically low signal level, the speed decreases in an avalanche-like manner (for example, to a level of 0.5 Mbit/s at a signal level of -117 dBm).

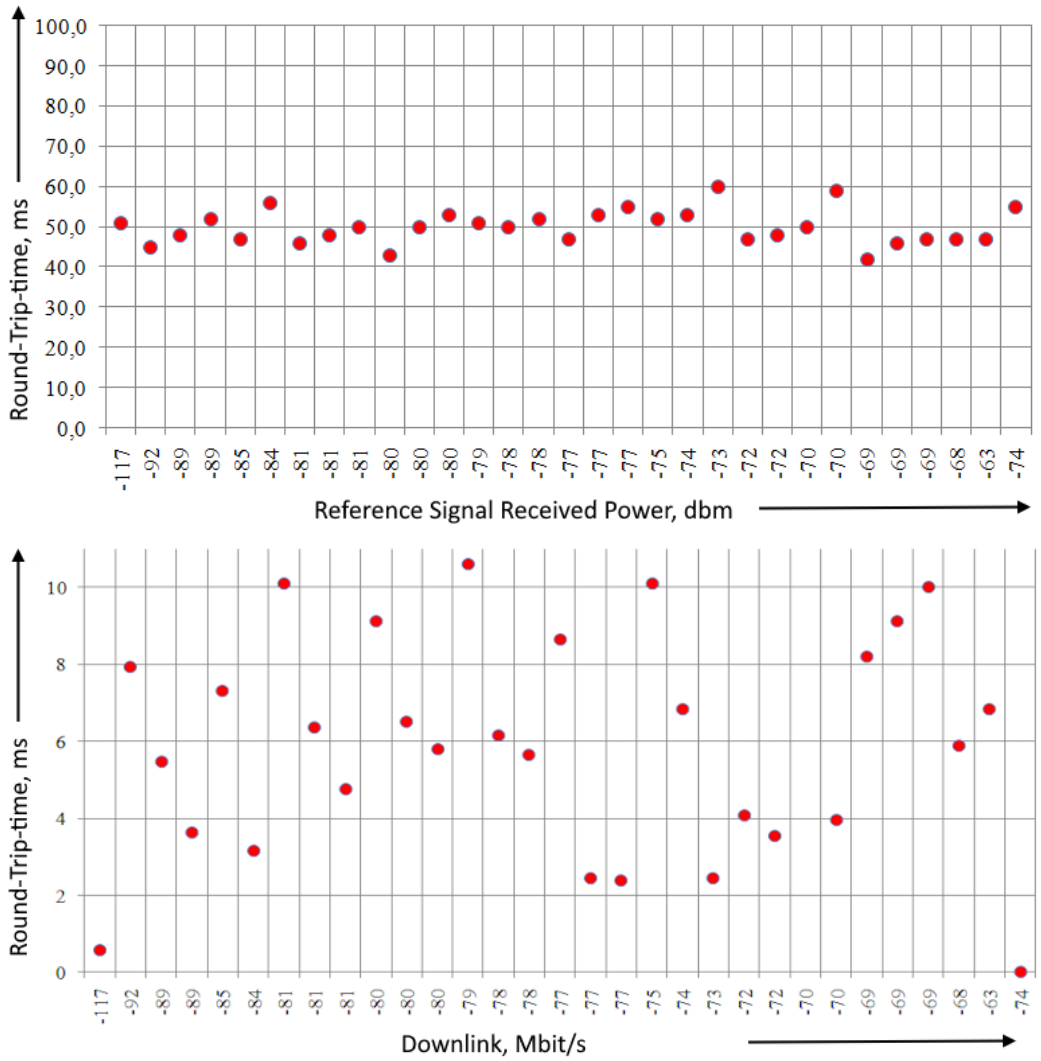

Fig. 5. Results of RTT and DLR measurements

VoIP-to-ISDN gateway based on IP PBX allows optimizing network traffic by adjusting of packet size depending on codecs. The most software based PBX's use RTP protocol for transport voice packets. There codecs G.711 (A-law for Europe and Russia and u-law for USA and Japan) and G.729 are most popular in software solutions of IP-PBX. They provide good call quality in various network conditions. For an example, G.729 requires low bandwidth and has proven to be effective when network resources need to be optimized. But G.711 consumes more bandwidth and provides high voice quality where bandwidth availability has been less of an issue [22, 23]. Solutions of IP-PBX allow a list of codecs for speech encoding and decoding; flexible numbers of subscriber and set of services, because IP-PBX should be able to extend and interact with other systems.

Codec's spec in VoIP-side of the gateway determines number of speech frames, overall packet length of RTP-packet and ratio of useful part of the package to the overall RTP packet length.

Calculating of speech frame numbers, overall RTP-packet length and ratio of useful part of the package to overall RTP packet length, for each codec (G.711, G. 726 (32kbit/s) and GSM) are possible due to choose one of the codecs in IP-PBX. It also possible to compare results of calculation with results from network analyzer.

To calculate the number of speech frames transmitted per second the formula is used:

$$n = \frac{1}{T_{sample}} \quad (1)$$

n – number of speech frames per second, frames/s; T_{sample} – duration of voice sample, s.

Voice sample duration depends on used encryption technology. The next step is to calculate the size of the packetized data according to the formula:

$$H = v \cdot T_{sample} \quad (2)$$

H – the size of packetized data, bytes; v – the encoding rate, bytes/s.

Encoding rate is calculated by the formula:

$$v = \frac{r}{8} \quad (3)$$

r – bit rate, bits/s.

Bit rate is different for each codec and depends on encryption technology. Headers of RTP and TCP/IP stack should be considered in order to determine full size of RTP packet. The total length of headers is 40 bytes (RTP – 12 bytes, UDP – 8 bytes, IP – 20 bytes). The total length of RTP packets encapsulated into stack UDP/IP is defined by sum of length of packetized data, IP-header, UDP header and RTP header:

$$H_{total} = H + H_{ipheader} + H_{udpheader} + H_{rtpheader} \quad (4)$$

Useful part ratio of the package to total size of RTP packet ratio for each codec is defined using the formula:

$$\mu = \frac{H}{H_{total}} \cdot 100\% \quad (5)$$

The parameter values for some of the codecs and calculation results are shown in the Table 2.

Table 2

Calculation results

Type of codec	Bit rate r , kbit/s	Duration of voice sample Tsample , ms	RTP packet size, bytes	μ, %
G.711 (A-law)	64	20	200	80
G.726 (32,0 kbit/s)	32	20	120	67
GSM	13	20	73	45
iLBC (13,33 kbit/s)	13,33	30	90	56
iLBC (15,2 kbit/s)	15,2	20	78	49
G.723.1	5,3	30	60	33
G.723.1	6,3	30	64	37
G.729 A	8	10	50	20
Silk	40	20	140	71

Thus, when G.711 codec is used for encoding speech on the VoIP area of LTE access to ISDN, voice is transmitted over 50 frames per second and packet size is 160 bytes. Each frame is encapsulated in the protocols RTP, UDP and IP, resulting in the packet size increases to 200 bytes, and useful part of the package is 80% of the total. It is possible to use, for example G.729 A with minimal RTP packet size, but ratio of useful parts for this codec is 20%.

Still, in the conditions of using LTE as an access network, it is important to take into account the operating conditions of the radio interface. Public wireless networks demonstrate excellent performance for VoIP in terms of throughput, packet loss, latency and jitter [24,25]. However, a closed LTE-R network requires QoS analyzing depending on radio coverage, electromagnetic compatibility, subscriber speed etc.

Conclusion

This article describes a method for creating a VoIP ISDN gateway over LTE using software and hardware solutions and the main aspects of implementing laboratory setup. An analysis of network boundary signaling for some communication scenarios is carried out. The laboratory facility can be integrated into existing railway communication networks as a diagnostic tool of operation analysis of LTE access in different conditions including interface disturbances.

The main advantage of the proposed gateway is based on existing hardware and freely licensed software. Analysis of the gateway operation in the LTE network showed that the quality of the wireless network is sufficient for its successful operation. Current work is continued as improving the gateway for performance experiments according QoS management and to improving system efficiency, bandwidth and LTE criteria.

REFERENCES

[1] Badach Anatol, “Voice over IP – Die Technik: Grundlagen, Protokolle, Anwendungen, Migration, Sicherheit, Notrufdienste, Videotelefonie,” 2022, DOI 10.3139/9783446471504.

[2] Suleiman Abdullahi, “Optimization of secured IPv4 and IPv6 unified VoIP network system with evaluation framework for SMEs (A comparative case study of YATE free PBX and 3CX phone system),” 2015. DOI 10.13140/RG.2.1.1225.5200

[3] Johanson Miserigodiasi Lyimo, “Implementing a campus VoIP intercom VLAN: A technology review, system requirements and architecture,” *International Journal of Science and Research Archive*. 2023. No. 9(2), pp. 716-726. DOI 10.30574/ijsra.2023.9.2.0648.

[4] M. Muthoharo, M. D. Atmadja, and A. Rasyid, “Analysis of Voice Quality on Aircraft Telephone Through Internet Telephony Gateway in Voice Over Internet Protocol,” *Jartel*. 2022.Vol. 12, No. 2, pp. 80-84. DOI 10.33795/jartel.v12i2.309

[5] Nader K. EL-Ashri, Ehab F. Badran, Amira I. Zaki, Waleed K. Badawi, “Admission control mechanism for quality of service and security in H.323 voice gateway,” *Concurrency and Computation: Practice and Experience*. 2021. Vol. 33, No. 20. DOI 10.1002/cpe.6376

[6] S. Barakovic, J. Baraković Husić, “Quality of Experience of Future ICT-based Logistics and Transport Systems,” *International conference on advances in traffic and communication technologies*, 2023, pp. 103-108. DOI 10.1080/02564602.2020.1786472

[7] Y. Sun, C. -Y. Lee, J. -m. Jo, J. -h. Lee and Y. -J. Han, "Study on the effectiveness of high-speed railway communication and signaling system based on 4G LTE technology," *2013 13th International Conference on Control, Automation and Systems (ICCAS 2013)*, Gwangju, Korea (South), 2013, pp. 402-406, DOI 10.1109/ICCAS.2013.6703988.

[8] M. Makni, M. Baklouti, S. Niar, M. Biglari-Abhari and M. Abid, "Heterogeneous multi-core architecture for a 4G communication in high-speed railway," *2015 10th International Design & Test Symposium (IDT)*, Amman, Jordan, 2015, pp. 26-31, DOI 10.1109/IDT.2015.7396731

[9] P. Fraga-Lamas, T. M. Fernández-Caramés, L. Castedo, “Towards the Internet of Smart Trains: A Review on Industrial IoT-Con- 1666 nected Railways,” *Sensors*, 2017, 17(6), No. 1457, 44 p. DOI 10.3390/s17061457

[10] Z. Kljaić, D. Pavković, M. Cipek, M. Trstenjak, T. J. Mlinarić, M. Nikšić, “An Overview of Current Challenges and Emerging Technologies to Facilitate Increased Energy Efficiency, Safety, and Sustainability of Railway Transport,” *Future Internet*. 2023; No. 15(11):347. DOI 10.3390/fi15110347

[11] Prashant Singh, Zeinab Elmi, Vamshi Krishna Meriga, Junayed Pasha, Maxim A. Dulebenets. Internet of Things for sustainable railway transportation: Past, present, and future. Cleaner Logistics and Supply Chain, 2022. Volume 4. ISSN 2772-3909. DOI 10.1016/j.clscn.2022.100065

[12] M. Chrzan, “Study of the possibility of using transmission in the LTE system on a selected rail-way line for the purpose of running rail-way traffic,” *Archives of Transport*, 2021. No. 57(1), pp. 91-101. DOI 10.5604/01.3001.0014.7486

[13] B. Allen et al., “Next-Generation Connectivity in A Heterogenous Railway World,” *IEEE Communications Magazine*, 2023. Vol. 61, No. 4, pp. 34-40. DOI 10.1109/MCOM.001.2200130

[14] Y. Kim, Y. Yoon, J. Kim, Y. Song, and S. W. Choi, “Functional Analysis between LTE-Railway and Public Safety-LTE,” *Journal of the Korean Society for Railway*, 2017 Vol. 20, pp. 20-30. DOI:10.7782/JKSR.2017.20.1.20

[15] Riefand Fadhlurrohman, Agung Triayudi, Ratih Titi Komala Sari, “VoIP System Implementation Using Issabel as an Integrated IP PBX Server with Telco Vendors. SaNa,” *Journal of Blockchain, NFTs and Metaverse Technology*, 2024. Vol. 1(2), pp. 56-64. DOI 10.58905/sana.v2i1.274
[16] H. Andrianto, D. Setiadikarunia, H. Raharjo, “Evaluasi Kinerja GSM VoIP Gateway pada System IP PBX,” *ELKOMIKA: Journal Teknik Energi Elektrik, Teknik Telekomunikasi, & Teknik*, 2021. Vol. 9, No. 3 DOI 10.26760/elkomika.v9i3.731
[17] Mullangi Pradeep, Shanmugam Kannan, Devi Kalasamudram, Paramasivan Kannan, Babu M, Mathew Cyril, Jaganpradeep J., and Nagalingam Rajeswaran, “Source Code Analysis on Asterisk VOIP IP PBX: An Open-Source Communication Toolkit,” *Tuijin Jishu/Journal of Propulsion Technology*, 2023. No. 44. 6768-6785. DOI 10.52783/tjjpt.v44.i4.2307
[18] E. J. Guaña Moya, A. P. Cabrera Sanmartín, R. D. Camacho Reyes, F. R. Marcillo Vera, “Configuración y gestión de equipos VOIP,” *Religación Press*, 2024 https://doi. org/10.46652/ReligacionPress.176
[19] J. Meggelen et al, “Asterisk – Future of telephony (Russian version),” Saint Petersburg: Simvol-Plus. 2009. 656 p.
[20] Data Sheet HFC-S 2BDS0. ISDN HDLC FIFO controller with S/T interface. Kologne: Kologne Chip Designs. 1997. 57 p.
[21] Actris. Multiprotocol Analyzer. Actris ptotokollmonitor workshop Version 1.0 5/99. Larmor Plage: Wawetel Telecommunication Test Solutions. 1999. 214 p.
[22] Amina Dallaf, “Optimizing SIP-Based VoIP Systems for LAN Infrastructures: Addressing Performance Demands and Quality Assurance in Wired and Wireless Environment,” *Journal of Electronics and Communication Engineering Research*, 2024. Vol. 10, pp. 15-27.
[23] Asmaa Jaish, Basim Al-Shammari, “Quality of experience for voice over internet protocol (VoIP),” *Wasit Journal of Engineering Sciences*, 2023. No. 11, pp. 96-105. DOI 10.31185/ejuow.Vol11.Iss3.460
[24] R. A. Putri, Anhar Anhar, Anggi Saputra, Rama Caniago, Rosarindo Harianja, “Analysis of 5G Network Quality of Service on VoIP Application,” *International Journal of Electrical, Energy and Power System Engineering*, 2024. No.7, pp. 37-45. DOI 10.31258/ijeepse.7.1.37-45
[25] Devi Gayathri, D. Sasikala, R. Srinath, M. Praveen, R. SureshKumar, Muthu Perumal, “Survey on VoIP transmission in 3GPP standards,” *International Journal of intelligent systems and applications in engineering*, 2024. No. 12 (21s), pp. 4221-4226.

SYNCHROINFO JOURNAL

www.media-publisher.eu/synchroinfo-journal

SOLVING THE PROBLEM OF SPEECH COMMANDS RECOGNITION

Chi Thien Nguyen [1]

[1] Ho Chi Minh City University of Technology (HCMUT), Ho Chi Minh City, Vietnam

ABSTRACT

In terms of technology development, speech recognition has a long history marked by several waves of major innovations. More recently, the field has been boosted by advances in deep learning and big data. These advances are evidenced not only by the growing number of scientific papers published in this area, but by the worldwide adoption of various deep learning methods in the design and implementation of speech recognition systems. The wide variety of speech signal processing tasks, as well as its high variability and instability of processing results in general, require a new formulation of the processing task in this area. Given staging tasks identification models speech production with purpose adequate perception. Researched solution tasks speech recognition teams. Tasks identification models of speech production with purpose adequate perception are presented and two adjustment schemes for speakers to improve speech recognition out signals. The transformation of speech signals and their recognition are implemented using likelihood functions. Given results experiments with proposed schemes under-construction sites. One hundred experiments were carried out on speech signals from the public access database TIDigits 1.0.

KEYWORDS: *chalk-frequency cepstral odds, recognition speeches, adjustment under announcer*

DOI: 10.36724/2664-066X-2024-10-4-43-50

Received: 17.06.2024
Accepted: 24.07.2024

Citation: Chi Thien Nguyen, "Solving the problem of speech commands recognition," *Synchroinfo Journal* **2024**, vol. 10, no. 4, pp. 43-50

Licensee IRIS, Vienna, Austria.

Introduction

Statement of the problem of speech production model identifying for the purpose of adequate perception. A wide variety of speech signal processing problems, as well as its high variability and instability of processing results in general, require a new statement of the processing problem in this area. In this problem, it is necessary to generalize the speech signal processing existing experience in order to improve of their processing quality [1-6]. Call this problem of identifying - the model of speech production for the adequate perception purpose.

According to the author, the problem of identifying the speech production model for the purpose of adequate perception should be solved in three stages.

Step 1 – identification. It is assumed that the speech signal is generated in accordance with some known model of speech production. Assuming that this model is parametric, it is necessary to estimate the values of its parameters for a given speech signal.

Step 2 – generation. If the model of the speech signal is identified, it is assumed that there is a generation mechanism that allows reproducing the corresponding speech signal. In this case, it is possible to vary the parameters of the model, achieving a change in the resulting speech signal.

Step 3 – adequate perception. It is assumed that the speech signal is perceived and interpreted. We will assume that a person or a group of persons (subjects) acts as the perceiving and interpreting device. In addition, the corresponding technical system can be used in this role. Assume that the perception of the speech signal is adequate if its meaning is recognized by the subjects (and/or the technical system).

It is easy to see that the task of identifying a speech generation model for the purpose of adequate perception has many common features with other tasks of speech technology: speech encoding at the first stage, parametric speech synthesis at the second stage, speech recognition at the third stage.

Thus, the stages of solving this problem mean performing a very specific generalized “procedure” of processing, the steps of which are determined by the stages considered above.

If the generated speech signal is adequately perceived, the procedure ends. Otherwise, it returns to the second step with a different set of model parameters.

Solution of the speech command recognition as a problem of identifying speech production model for the adequate perception purpose

Automatic speech recognition systems based on multiple speakers for stable recognition are divided into speaker-dependent and speaker-independent. The term "speaker-independent" means that the accuracy for a given user is close to the average accuracy taken for all possible speakers. But creating a truly speaker-independent system is a very labor-intensive task, since a large amount of training data is required. At the current stage of speech recognition system development, the error rate in speaker-independent systems is 3-5 times higher than in speaker-dependent systems. At the same time, a speaker-dependent system will recognize words with the accuracy of recognizing words of "its" user (the person who trained this system), which will be higher than the accuracy taken for "foreign" users. Therefore, to improve the quality of speech command recognition in the case of a "foreign" user, it is proposed to transform the speech signals of the "foreign" user to the speech signals of "its" user before sending the signal to the input of the recognition algorithm. This idea is found in [7], where transformation and recognition are performed using distance functions. In this paper, transformation of speech signals and their recognition are implemented using likelihood functions. Below are two speaker-tuning schemes for improving recognition of their speech signals.

First scheme. Let the signal $Y = (y_1, y_2, \dots y_T)$ mean the pronunciation of some speech command. The value of T is an integer, positive. Let us call the set of different pronunciations of the same command a class. Let K speech commands be used, i.e. K signal classes $j = 1,2,\dots,K$. Let the speech signal Y be pronounced by some "foreign" user, different from "own" user. It is necessary to decide to which class the speech signal Y belongs. To construct a decision rule, the speech signals of "own" user are specified with an indication of the class.

Thus, the problem can be solved by the following "algorithm".

Step 1 – Identification. The speech signal itself is characterized by great variability. In practice, the speech signal is presented as a more stable characteristic (a sequence of feature vectors) to improve the quality of its classification. Features can be different. The most popular features are small-frequency cepstral coefficients [8, 9]. The sequence of feature vectors is denoted by $X = (\mathbf{x}_1,\mathbf{x}_2,\ldots,\mathbf{x}_\tau)$, where – $\mathbf{x}$ is the feature vector. In the general case, the length of the sequence of feature vectors is not equal to the length of the speech signal $\tau \neq T$. We will consider the signal X as a model of the speech signal Y of an "alien" user.

Step 2 – Generation. Considering the model X as parametric $X = X^{(a)}$, we vary it using the parametric family of functions $\varphi(X,a)$ for different values of the parameter $a \in R$. We obtain a new model $\tilde{X}^{(a)} = \phi(X, a)$.

Step 3 – Adequate perception. The speech command recognition system with a decision rule, which is built on the speech signals of "its" user, is used as the perceiving and interpreting one.

We will consider a Bayesian classifier with a decision rule of the form

$$p_j = \arg\max_j p(X \mid j)p(j),\ j = 1,2,...,K.$$

Let the a priori probabilities of classes $p(j)$ be equal for all j = 1,2,...,K. Then the decision rule is simplified:

$$p_j = \arg\max_j p(X \mid j),\ j = 1,2,...,K.$$

To estimate the distribution densities $p(X \mid j)$, speech signals of "one's" user with an indication of the class are used [10].

Since at steps 1 and 2 (identification and generation) a model $\tilde{X}^{(a)}$ of the original speech signal Y is obtained, the decision rule takes the following form

$$p_j = \arg\max_j p(\tilde{X}^{(a)} \mid j),\ j = 1,2,...,K.$$

For the presented problem, the concept of adequate perception is specified as follows. We will estimate the quality of perception by probability $\max_j p(\tilde{X}^{(a)} \mid j),\ j = 1,2,...,K.$ Perception is adequate when the assessment $\max_j p(\tilde{X}^{(a)} \mid j),\ j = 1,2,...,K$ reaches a maximum for some value $a \in R : \max_a \max_j p(\tilde{X}^{(a)} \mid j),\ j = 1,2,...,K,\ a \in R.$

If the speech signal is adequately perceived, the algorithm ends. Otherwise, it returns to step 2 with a different parameter a. The final solution is

$$p_j = \arg\max_a \max_j p(\tilde{X}^{(a)} \mid j),\ j = 1,2,...,K,\ a \in R.$$

Let us consider the problem of identifying a model X as a sequence of vectors of mel-frequency cepstral coefficients of a signal Y. Mel-frequency cepstral coefficients are based on two key concepts: cepstrum and mel-scale. Cepstrum is the result of a discrete cosine transform from the logarithm of the amplitude spectrum of signal Y in a certain window. The mel-scale models the frequency sensitivity of human hearing. Psychoacoustics experts have found that a twofold change in frequency in the range of low and high frequencies is perceived differently by humans. In the frequency band up to 1000 Hz, the subjective perception of frequency doubling coincides with a real doubling of frequency, therefore, up to 1000 Hz, the mel-scale is close to linear.

For frequencies above 1000 Hz, the mel-scale is logarithmic. The conversion from the hertz scale to the mel-scale is performed using the formula $f_{Mel} = 1127 \ln(1 + \frac{f_{Hz}}{700})$. Mel-frequency cepstral coefficients *x* are the cepstrum values distributed according to the Mel scale [8].

It is believed that to characterize speech sounds it is sufficient to distinguish three formants – FI, FII, FIII, which are numbered in order of increasing frequency. A formant is a fairly clearly distinguished area of amplified frequencies, determined by the average frequency in the amplitude spectrum of the sound (Fig. 1). The average distance between formants depends on the characteristics of the speaker's voice (the distance for females is somewhat greater than for males) [11]. Thus, the transformation function φ(*X*, *a*) is available to us as the function φ(*A*, *a*), where − *A* is the amplitude spectrum, which is an intermediate value in the process of extracting the model *X* from the original signal *Y*.

It is desirable that the amplitude spectrum be expanded if *a* < 1, and compressed if *a* > 1. Recall that the amplitude spectrum is a function of the angular frequency *A* = ξ(ω), where the normalized frequency is ω ∈ [0,π] [8]. The effect of spectrum expansion (compression) can be achieved by simple distortion of the frequency axis $\tilde{\omega} = a\omega.$. The expanded (compressed) spectrum is determined by the expression $\tilde{A} = \xi(\tilde{\omega})$. Then the new frequency $\tilde{\omega}$ takes values in the range from 0 to *a*π. In order to eliminate this drawback, we will distort the frequency axis as follows:

$$\tilde{\omega} = \begin{cases} a\omega, \omega \le b, \\ ab + \dfrac{\pi - ab}{\pi - b}(\omega - b), \omega > b, \end{cases}$$

where – *b* is an additional parameter. The parameter *b* must satisfy the conditions

$$\begin{cases} 0 < b < \pi \ \text{ при } a < 1, \\ 0 < b < \dfrac{\pi}{a} \ \text{ при } a > 1. \end{cases} \quad (1)$$

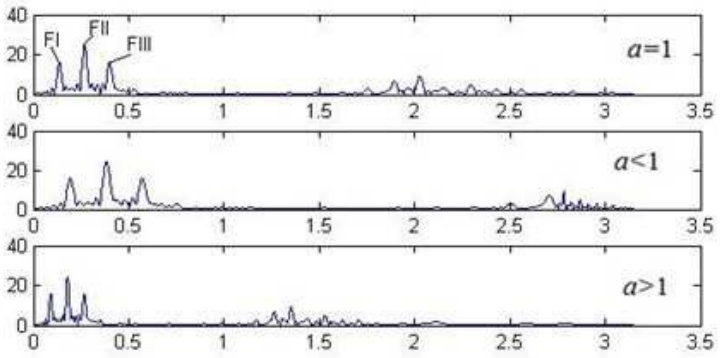

Fig. 1. Amplitude spectrum for various values *a*

The range of values of the parameter *b* is shown in Figure 2. In this paper, we will select the value of the parameter $b = \frac{7\pi}{8}$, if *a* < 1, and $b = \frac{7\pi}{8a}$, if a > 1, taking into account condition (1). The choice of such values of the parameter b is due to the need to change the distribution spectrum of the main formants, without paying attention to the rest of the spectrum of the speech signal in the range of the normalized frequency ω from 0 to π.

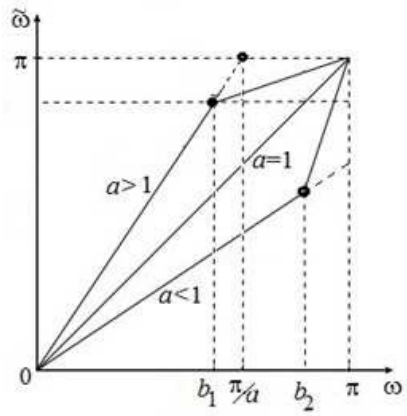

Fig. 2. Frequency axis distortion function taking into account the parameter *a*:
b_1 is the value of the parameter *b* for $a > 1$, b_2 for $a < 1$

Taking into account the distribution of human voice formants [12], it is impossible to expand (compress) the amplitude spectrum more than 2 times. Therefore, it is possible to select the value of the parameter a in the range from 0.5 to 2.

Second scheme. In the first scheme, it is required, when the next speech signal $Y_i, I = 1,2,\ldots$, appears, to determine its belonging to one of the classes $j = 1,\ldots,K$. In the second scheme, we assume that N speech signals are observed, pronounced by only one "foreign" user (it does not matter which one). It is necessary to classify these signals.

The problem can be solved using the following "algorithm" (scheme 2).

Step 1 – Identification. We obtain models $X_i, I = 1,2,\ldots,N$ of speech signals $Y_i, I = 1,2,...,N$ of the "foreign" user.

Step 2 – Generation. We vary the models $X_i, I = 1,2,\ldots,N$ using the parametric family of functions $\varphi(X,a)$ for different values of the parameter $a \in R$. We obtain new models $\tilde{X}_i^{(a)} = \phi(X_i, a), i = 1,2,...,N, a \in R.$

Step 3 – Adequate perception. The speech command recognition system with a decision rule built on the speech signals of "its" user is used as the perceiver and interpreter.

For the presented problem, the concept of adequate perception is specified as follows. We estimate the quality of perception by the sum of probabilities $\sum_{i=1}^{N} \max_j p(\tilde{X}_i^{(a)} \mid j), j = 1,2,...,K.$ Perception is adequate when the estimate reaches a maximum for some value $a \in R : \max_a \sum_{i=1}^{N} \max_j p(\tilde{X}_i^{(a)} \mid j), j = 1,2,...,K, a \in R.$

If the speech signals are adequately perceived, the algorithm ends. Otherwise, it returns to step 2 with a different parameter *a*. To optimize the function of the quality of perception from the parameter a, the "golden section" method [13] is used:

$$p_j = \arg\max_a \sum_{i=1}^{N} \max_j p(\tilde{X}_i^{(a)} \mid j), j = 1,2,...,K, a \in R.$$

The final solution is as follows

$$p_j = \arg\max_j p(\tilde{X}_i^{(a)} \mid j), j = 1,2,...,K, \; i = 1,2,...,N.$$

Experiments

One hundred experiments were conducted on speech signals from the publicly available TIDigits 1.0 database [14-17]. First, one female voice was considered as the voice of "our" user, on whose speech signals a speaker-dependent speech recognition system with a decision rule for classifying 11 speech commands was built (we will call such a processing system a standard scheme). One "foreign" user pronounced 11 speech commands twice. The received speech signals of this "foreign" user were classified using the standard scheme. Then these signals were transformed and classified according to scheme 1 and scheme 2. The accepted class of each speech signal according to each scheme was compared with its true class. For each scheme, the frequency of correct recognition $v = \frac{N - N_r}{N}$ was determined, where − N is the total number of pronounced speech commands; N_r is the number of erroneously recognized ones. Such experiments were conducted with other "foreign" users. A group of 50 users (25 men, 25 women) played the role of an alien user. The results of the experiments are shown in Figure 3.

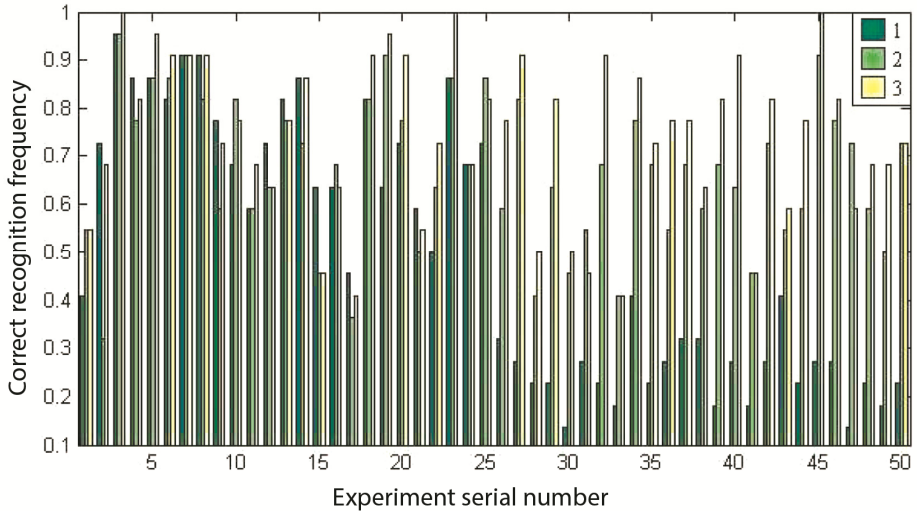

Fig. 3. Results of experiments where the "own" user is a woman:
1 – according to the standard scheme; 2 – according to scheme 1; 3 – according to scheme 2

The remaining 50 experiments were conducted like the first 50 experiments, except that the role of "own" user was played by one male voice. The results of the experiments are shown in Figure 4.

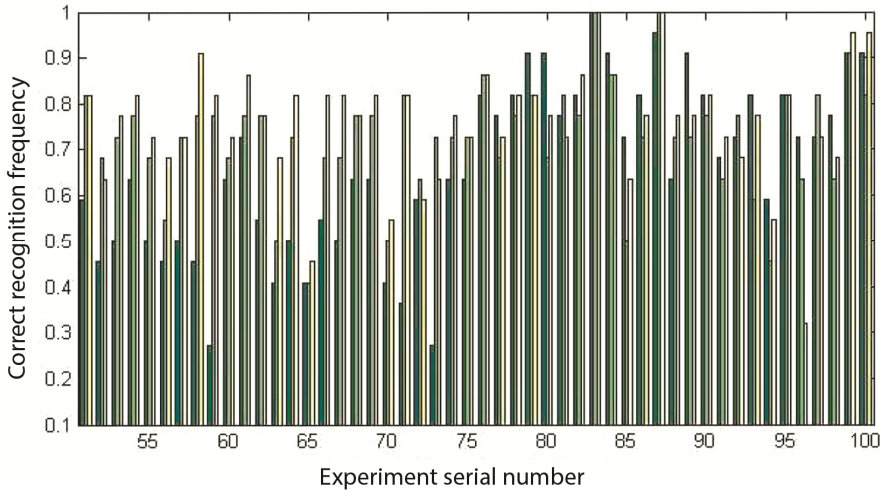

Fig. 4. Results of experiments where the "own" user is a man

The hypothesis was tested that the proposed schemes improve the recognition result compared to the standard scheme. For testing, the criterion of the arithmetic mean $\overline{v}$ of the frequencies of correct recognition *v* in experiments was used.

Based on the results of 100 experiments, it turned out:

– for the sta dard scheme $\overline{v}$ = 0.5755;

– for sche e 1 $\overline{v}$ = 0.6964;

– for sche e 2 $\overline{v}$ = 0.7510.

Consequently, it can be stated that schemes 1 and 2 improve the recognition result. It was noted that the quality of recognition depends on the difference or coincidence of the genders of one's own and another's users.

Based on the results of 50 experiments, where the gender of one's own user differs from the gender of another's user, it turned out:

– for the sta dard scheme $\overline{v}$ = 0.5309;

– for sche e 1 $\overline{v}$ = 0.69;

– for sche e 2 $\overline{v}$ = 0.7465.

Based on the results of 50 experiments, where the gender of one's own user coincides with the gender of another's user, it turned out:

– for the sta dard scheme $\overline{v}$ = 0.62;

– for sche e 1 $\overline{v}$ = 0.7027;

– for sche e 2 $\overline{v}$ = 0.7555.

For the standard scheme, the value of $\overline{v}$ in cases of coincidence of genders is significantly better than in cases of difference of genders (0.62 – 0.5309 = 0.0891).

In the proposed schemes, these values are approximately equal (0,6900 ≈ 0,7027 and 0,7464 ≈ 0,7555). Therefore, it can be argued that the use of the proposed schemes eliminates the influence of gender on the recognition result.

Conclusion

The paper proposes two speaker-tuning schemes to improve the quality of speech signal recognition. Experiments confirm the improvement in recognition quality. At the same time, the effect of eliminating speaker's gender influence on the recognition result is achieved. However, the average frequency of correct recognition is still far from satisfactory for practical speech command recognition systems (more than 95% is required). To improve the recognition quality, it is necessary to propose a more complex speech signal conversion function.

REFERENCES

[1] G. K. Berdibayeva, A. N. Spirkin, O. N. Bodin and O. E. Bezborodova, "Features of Speech Commands Recognition Using an Artificial Neural Network," *2021 Ural Symposium on Biomedical Engineering, Radioelectronics and Information Technology (USBEREIT)*, Yekaterinburg, Russia, 2021, pp. 0157-0160, doi: 10.1109/USBEREIT51232.2021.9455111.

[2] Daniel-S. Arias-Otalora, Andrés Florez, Gerson Mellizo, C. H. Rodríguez-Garavito, E. Romero, J. A. Tumialan, "A Machine Learning Based Command Voice Recognition Interface", *Applied Computer Sciences in Engineering*, vol.1685, pp.450, 2022.

[3] A. R B, V. R C, V. K, S. Chikamath, N. S R and S. Budihal, "Limited Vocabulary Speech Recognition," *2024 3rd International Conference for Innovation in Technology (INOCON)*, Bangalore, India, 2024, pp. 1-5, doi: 10.1109/INOCON60754.2024.10511500.

[4] A. Kuzdeuov, S. Nurgaliyev, D. Turmakhan, N. Laiyk and H. A. Varol, "Speech Command Recognition: Text-to-Speech and Speech Corpus Scraping Are All You Need," *2023 3rd International Conference on Robotics, Automation and Artificial Intelligence (RAAI)*, Singapore, Singapore, 2023, pp. 286-291, doi: 10.1109/RAAI59955.2023.10601292.

[5] Aditya Kulkarni, Vaishali Jabade, Aniket Patil, "Audio Recognition Using Deep Learning for Edge Devices", *Advances in Computing and Data Sciences*, vol.1614, pp.186, 2022.

[6] A. Yasmeen, F. I. Rahman, S. Ahmed and M. H. Kabir, "CSVC-Net: Code-Switched Voice Command Classification using Deep CNN-LSTM Network," *2021 Joint 10th International Conference on Informatics, Electronics & Vision (ICIEV) and 2021 5th International Conference on Imaging, Vision & Pattern Recognition (icIVPR)*, Kitakyushu, Japan, 2021, pp. 1-8, doi: 10.1109/ICIEVicIVPR52578.2021.9564183.

[7] N. G. Zagoruiko, V. S. Lozovsky, “Adjustment to the speaker in recognizing a limited set of oral commands,” *Collection of works of the Institute of Mathematics SB USSR Academy of Sciences*. No. 28. 1967.

[8] J. Benesty et al., “Handbook of speech processing,” Springer. 2008.
[9] Md. Rakibul Hasan, Md. Mahbub Hasan, Md Zakir Hossain, "How many Mel - frequency cepstral coefficients to be utilized in speech recognition? A study with the Bengali language", *The Journal of Engineering*, vol.2021, no.12, pp.817, 2021.
[10] A. V. Agranovskiy, “Theoretical aspects of algorithms for processing and classifying speech signals,” Moscow: Radio and communication, 2004. 162 p.
[11] S. V. Kodzasov, O. F. Krivnova, “General phonetics,” Moscow: Publishing house RSUH, 2001. 592 p.
[12] J. Hillenbrand et al., “Acoustic characteristics of American English vowels,” *The Journal of the Acoustical Society of America*, no. 97(5). 1995, pp. 3099-3111.
[13] D. G. Matthews, Numerical methods,” Using MATLAB, 3rd edition. Moscow: Williams Publishing House, 2001. 720 p.
[14] G. Leonard, G. Doddington, “TIDigits,” Linguistic Data Consortium, Philadelphia, 1993. URL: https://catalog.ldc.upenn.edu/LDC93S10 (date of access: 23.03.2024).
[15] H. Aghakhani et al., "Venomave: Targeted Poisoning Against Speech Recognition," *2023 IEEE Conference on Secure and Trustworthy Machine Learning (SaTML),* Raleigh, NC, USA, 2023, pp. 404-417, doi: 10.1109/SaTML54575.2023.00035.
[16] L. Guo et al., "Transformer-Based Spiking Neural Networks for Multimodal Audiovisual Classification," *IEEE Transactions on Cognitive and Developmental Systems*, vol. 16, no. 3, pp. 1077-1086, June 2024, doi: 10.1109/TCDS.2023.3327081.
[17] S. Xiang et al., "Neuromorphic Speech Recognition with Photonic Convolutional Spiking Neural Networks," *IEEE Journal of Selected Topics in Quantum Electronics*, vol. 29, no. 6: Photonic Signal Processing, pp. 1-7, Nov.-Dec. 2023, Art no. 7600507, doi: 10.1109/JSTQE.2023.3240248.

CERAMIC MATERIALS IN RADIO ELECTRONICS

Artem Dymkov [1]

[1] Institute of Radio and Information Systems (IRIS), Vienna, Austria
Dymkov@media-publisher.eu

ABSTRACT

The development of radio electronics, increasing reliability, reducing the dimensions and weight of devices is closely related to the development, study of properties and application of new materials. These include new ceramic and composite materials that can withstand high temperatures and successfully operate in aggressive environments. Ceramic materials are very diverse, each of them has its own unique chemical properties. They are very widely used in radio electronics and are promising for the development and improvement of designs of radio electronic devices. At present, industrial progress requires electronics to constantly increase the level of power, efficiency, reliability and durability. For modern devices, reliability under high currents and high temperatures is a key factor. The article analyzes the properties and advantages of various ceramic materials, their areas of application in radio electronics, and identifies promising areas of use.

DOI: 10.36724/2664-066X-2024-10-4-51-62

Received: 14.07.2024
Accepted: 20.08.2024

Citation: Artem Dymkov, "Ceramic materials in radio electronics," *Synchroinfo Journal* **2024**, vol. 10, no. 4, pp. 51-62

KEYWORDS: *ceramic materials, radio electronics devices, materials and components of radio electronics*

Introduction

Radio electronics development at the present stage, increasing reliability, reducing the dimensions and weight of devices are closely related to study of properties and application of new materials. These include new ceramic and composite materials that can withstand high temperatures and successfully operate in aggressive environments. They are promising for the development and improvement of radio electronic devices designs.

A fairly wide range of inorganic dielectric materials used in technology is represented by ceramic products. In the mid-1920s, the first capacitors using ceramics as a dielectric appeared in Germany. This happened due to a shortage of mica and experience in the production of porcelain - a special class of ceramics.

Paraelectric titanium dioxide (rutile) was used as the first ceramic dielectric. In 1926, these ceramic capacitors were produced in small quantities, and in the 1940s their number increased. In 1944, Soviet scientist B. M. Vul first synthesized a piezoceramic material, discovering the ferroelectric properties of barium titanate $BaTiO_3$.

Modern radio ceramics are characterized by: high heat resistance, non-hygroscopicity, good electrical insulation properties, mechanical strength, stability over time and resistance to external influences.

Ceramics: properties and advantages

Ceramics are materials obtained by sintering granular or powdered inorganic substances. They are multiphase structures containing crystalline, amorphous, and gas phases. The properties of ceramics depend on their chemical and phase composition, macro- and microstructure, and manufacturing technology.

Advantages of ceramics: high heat resistance, good and varied dielectric properties, and relatively high thermal conductivity.

In electronics, ceramics are used to manufacture insulating parts: support insulators, bases, housings for vacuum and semiconductor devices, housings, and substrates for microcircuits; capacitor ceramics are used in capacitors [1-3].

Ceramics are a multiphase system, the main phases of which are crystalline and glassy. The crystalline phase determines the electromechanical properties, and the glassy phase determines the manufacturing process of the parts.

In composition, all capacitor materials are mixtures of titanates, zirconates, and stannates of different metals. These compounds are classified as ferroelectrics by their electrical properties.

Ceramics are non-metallic polycrystalline materials (usually obtained by sintering powders), while sintering is only one of the methods (traditional) for obtaining ceramics; crystallization, impact pressing and other methods of obtaining it can be used:

– non-metall c ceramics are oxides, carbides, nitrides, etc.;

– polycrystalline ceramics are many micron-sized grains (otherwise – the field of nanomaterials);

– co rse ceramics (5-30% pores) – building materials, refractories;

– high y porous ceramics (~30% pores) – thermal insulation materials;

– fine ceramics (artistic – porcelain, earthenware) and functional (piezo-, ferro-, magnetic, thermoelectric, superconducting, insulating, optical, etc.).

Ceramics are not: pressed metal powders, glass and amorphous materials, aerogels, sitalls, glass wool, asbestos, single crystals, pressed granular plastics.

The properties of ceramics are determined by the physical properties of crystallites, the size and shape (anisotropy, etc.) of crystallites, the nature of the bond between crystallites, the presence of pores, liquid phases, etc.,

The manufacture of ceramic products is a very complex process, during which it is necessary to ensure a given chemical and mineralogical composition of ceramics, minimize the content of the gas phase and achieve the required accuracy of the dimensions of the products.

The production process begins with the preparation of a mass, the components of which are selected by composition, ground and mixed in ball mills to achieve homogeneity. From the resulting mass, blanks of products are made by one of the methods:

– pr ssing dry powder - when making small flat products;

– forming on a potter's machine or in plaster molds – for products of large sizes and a fairly complex shape;

– extrusion through a mouthpiece or drawing with subsequent mechanical processing – for elongated produ ts (tubes, rods, frames, blocks, etc.);

– stampi g – for mass-produced products of various configurations;

– casting of liquid mass into special molds – in the manufacture of large-sized products of complex configurations.

A mandatory operation of the technological process is the firing of blanks – the most important operation, since the firing time, temperature and composition of the environment (oxidizing, reducing) determine the final suitability of the product. Firing is carried out in tunnel kilns with a strictly specified temperature gradient and careful observance of the speed of movement. To improve the quality appearance, mechanical strength and electrical insulation properties of the product, they are sometimes glazed. To ensure the possibility of soldering, metallization of ceramics is carried out by burning in silver.

Ceramic dielectric materials are divided into passive and active. The most widely used passive ceramics are materials with a crystalline phase of the BaO Al_2O_3 SiO_2 system. These include radioporcelain, aluminoxide, ultraporcelain, corundum-mullite and Celsian ceramics [4]. Passive ceramics are divided into installation and capacitor ceramics according to their purpose and electrical properties.

Installation ceramics must have $\varepsilon < 10$, increased mechanical strength and good electrical insulation properties. It is used to manufacture support, feedthrough, suspension insulators, lamp panels, coil frames, and radio tube parts. Most types of installation ceramics are high-frequency dielectrics and have tg $\delta \sim 2 * 10^{-3}$ at a frequency of 1 MHz.

Capacitor ceramics are used to manufacture high- and low-voltage capacitors and are divided into ceramics with increased (more than 12) and high (more than 900) dielectric constant ε.

Materials for high-frequency capacitors have moderate and increased permittivity *r* = 14…250, normalized value of temperature coefficient, which can be both positive and negative or close to zero, small tg $\delta \sim 10^{-4}$ (tg of dielectric loss angle β), high electrical strength. Some types of ceramics belong to the class of active dielectrics, the properties of which depend on external influences and are used mainly as ferroelectrics and piezoelectrics.

Insulating products for radio-electronic systems (RES) are currently obtained from high-alumina ceramics (more than 94% alumina Al_2O_3). During firing of the workpiece, a modification of alumina is formed – Al_2O_3, called corundum.

There are two known brands of corundum ceramics: VK94-1 and Polikor. The first is the main material for housings of semiconductor devices and microcircuits. Polikor contains at least 99.7% – Al_2O_3 and can be obtained transparent, since it has virtually no pores, and the structure is fine-crystalline. These materials have a moderate permittivity *r* = 9...10, very small tg110^{-4}, a fairly high thermal conductivity coefficient about 20...30 W/(m*K), a temperature coefficient of linear expansion l = (4 ... 6) 10^{-6} K^{-1}.

Ceramics on beryllium oxide BeO, called "brokerite", have a significantly higher thermal conductivity (~200 W/(m*K)) and good dielectric properties. It is used for substrates and housings of powerful microcircuits and semiconductor devices. A feature of brokerite is a low coefficient of linear expansion: l = 1.410^{-6} K^{-1}.

Even higher than that of brokerite, the thermal conductivity of diamond heat-conducting ceramics: = 500 W/(m*K), which is more than that of silver and copper. Such ceramics are made by sintering small crystals of synthetic diamonds. Despite the high cost, diamond ceramics are used in powerful semiconductor devices for special purposes.

Structural ceramic materials are divided into two groups: oxide ceramics (including silicates and glass ceramics) and oxygen-free (carbides, nitrides, borides). For a long time, materials scientists did not consider ceramics as a possible structural material. This was due to its main drawback – brittleness. But in other key performance parameters (heat resistance, hardness, corrosion resistance, density, availability and cheapness of raw materials) it significantly surpasses metals and alloys (Table 1).

Table 1

Ceramic materials types for electronics industry

Ceramic materials classification by purpose	Ceramics properties	Ceramic material name
Dielectrics		
Ceramics for installation products and small-capacity capacitors (high-frequency dielectrics)	Low permittivity (ε < 10); low dielectric losses (tgδ) at a frequency of 10^6 Hz; high values of: specific volume resistance, mechanical strength, breakdown voltage	Soapstone, ultraporcelain, corundum, celsian, corundummullite, forsterite, cordierite, bromellite ceramics
Capacitor ceramics		
For high-frequency circuit capacitors, including temperature-compensating and separating capacitors	High dielectric constant, negative temperature coefficient of permittivity (TKε)	Rutile ceramics (tikond T-80); perovskite ceramics – T-150 (based on $CaTiO_3$)
For high frequency thermally stable capacitors	Low value TK $\varepsilon \approx 0$	Titanium-zirconium ceramics (T-20, T-40); stannate ceramics C-15 (having a crystalline phase in the form of solid solutions of calcium stannate $CaSnO_3$, calcium titanate $CaTiO_3$ and calcium zirconate $CaZrO_3$); $CaTiO_3$ – $LaAlO_3$; TL-47*, TL-75*
For low frequency capacitors (linear)	Very high dielectric constant (ε<300)	SVT – strontium-bismuth titanate $SrTiO_3 \cdot Bi2O_3 \cdot 2NiO_2$
Porous ceramics (high temperature insulation)		
For electron tubes insulators	Low loss tangent value	Porous corundum and porous steatite ceramics
For bases of wire resistances (resistors)	High thermal resistance	Chamotte, alundum (sintered corundum), cordierite ceramics
For low frequency capacitors	Ultra-high dielectric constant (reaching several thousand)	SM-1, T-7500**, T-10000**, materials based on $BaTiO_3$
For piezoelectric elements	High piezoelectric modulus value	T-1700, zirconate – lead titanate $PbZrO_3$ – $PbTiO_3$
For nonlinear elements	Sharp dependence of permittivity on electric field strength	Variconds
Semiconductors *Semiconductor ceramics (high electronic conductivity)*		
For high power radio resistors, waveguide loads, high temperature heaters	Low dependence of resistance on temperature and voltage	Ceramics based on silicon carbide, as well as containing graphite (silite, kerax)
For nonlinear elements (varistors)	Sharp resistance versus voltage dependence	Ceramics based on silicon carbide (vilite, NPS based on ZnO with additives)
For thermal resistances (thermistors and posistors)	Sharp dependence of resistance on temperature	Ceramics based on copper and cobalt-manganese reverse spinels
Magnetic ceramics *(high magnetic permeability with high electrical resistance)*		
Magnetically soft	Low coercivity value	Nickel-zinc, manganese-zinc, magnesium and other ferrites
Magnetically hard	High coercivity value	Barium ferrites

* The number indicates the temperature coefficient of capacitance $\times 10^{-6}$;** The number usually indicates the value of permittivity; T – titanate.

Designations:
- TiO_2, ZrO_2 (YSZ, stabilization with yttrium or calcium oxides);
- Titanates, zirconates, niobates, tantallates Ba, Sr, Pb, K, Na, lead titanate-zirconate (PZT) – high density, required permittivity and loss tangent (piezoelectronics and radio engineering);
- ZrO_2 – ionic conductivity and oxygen sensors;
- Al_2O_3, MgO, SiO_2 – electrical insulation;
- Spinels, ferrites Ni, Co, Mn, Ca, Mg, Zn, Li – magnetic circuits, cores, memory devices;
- $MoSi_2$, resistance ~200 μOhm*cm, stability in an oxidizing atmosphere up to 1650 °C – electric heaters;
- perovskites (and intergrowth structures) $REEBa_2Cu_3O_7$;
- $Bi_2Sr_2CaCu_2O_8$ (2212, 2223) – current leads, limiters of maximum permissible current, superconducting tapes, solenoids, magnetic levitation;
- MgB_2 – electric heaters;
- Al_2O_3, SiO_2 – thermal insulation;
- SiC, Si_3N_4 – in the reaction chamber;
- SiC, Al_2O_3 – reaction limiters,
- Al_2O_3, BeO – reaction chamber windows;
- Al_2O_3, MgO, SiO_2 – electrical insulation;
- UO2, UC, UN, PuO_2 – nuclear fuel;
- SiC, Si_3N_4 – fuel element cladding;
- BeO, ZrO_2, Be_2C – neutron moderators and reflectors;
- B_4C, HfO_2, Sm_2O_3 – neutron shielding.

The increased susceptibility of ceramics to brittle fracture is associated with the extremely low mobility of defects, caused primarily by the specific (ionic-covalent) nature of the bond in ceramic structures. Therefore, the efforts of researchers are aimed primarily at eliminating such microscopic defects in ceramics that act as centers for crack initiation. One way to achieve this goal is to thoroughly clean and very finely grind the original powder and pack it tightly before sintering. The idea of using fine grinding of powders to intensify sintering was first put forward in Russia by Academician P.A. Rebinder back in the 1950s.

Hot pressing produces the most highly durable materials from silicon carbide, but products made from them are more expensive than those obtained by other methods, which is due to the impossibility of manufacturing parts of complex configurations without expensive mechanical processing with a diamond tool.

In the near future, fundamentally new ceramic materials are expected to be used [16]. An example is the superplastic ceramics obtained relatively recently in Japan based on the tetragonal modification of zirconium dioxide doped with 3 mol. % yttrium oxide.

Under specific conditions of raw material preparation and sintering, a polycrystalline material with a crystallite size of 0.3 μm is obtained, which is capable of deformation, stretching under external loads twice as much as the original length. It is characteristic that after such stretching, the ceramics have a strength exceeding the strength of silicon nitride, which is considered the most promising structural material.

Substrates based on beryllium oxide (BeO), although they have excellent heat-conducting properties and high electrical resistance, are expensive and very toxic. They are still indispensable in the manufacture of microwave transistors, since their losses at high frequencies are very low [12-14]. But here, too, in the production of devices based on SiC, a more promising solution is outlined. If the transistor or diode has a planar design, the thinnest AlN film grown on the back side of the SiC substrate provides reliable insulation due to its high breakdown voltage, practically not hindering heat dissipation. Operation of SiC semiconductor devices at temperatures above 200-250°C is impossible even on BeO substrates due to the significant difference in the coefficient of linear expansion.

Therefore, today the most popular product on the SiC device market is silicon carbide substrates. Their quality improves and their diameter increases every year. Now it is 100 mm.

Thus, new ceramic materials are promising for the manufacture of housings for electronic modules and substrates for printed circuit boards that experience high thermal and mechanical loads [6-10]. The development of these designs will help reduce both the dimensions and weight of products, and increase reliability and energy efficiency.

Examples of ceramic materials

The use of ceramics in technical applications is not only not decreasing, but also increasing, moving towards simplifying industrial processes with a simultaneous increase in manufacturability [11].

Examples of ceramic materials used in radio electronics:

Steatite ceramics. Talc serves as the basis for its production. Such ceramics are used to make mounting elements, terminals, stands, bobbins, switches, and axes for variable capacitors.

Forsterite ceramics. Magnesium orthosilicate serves as its basis. The material has low dielectric losses, good high-frequency characteristics, and high resistance even at high temperatures. Forsterite ceramics are used to make resistors, microcircuits, transistors, diodes, and terminals.

Alumina ceramics. It is produced by sintering alumina powder. The material has high mechanical strength (280-350 MPa for bending), hardness (9 on the Mohs scale), and abrasion resistance. Alumina ceramics are used to manufacture microcircuits, microcircuit housings, boards for film resistors and diodes, terminals that are resistant to high temperatures.

Aluminum nitride (AlN). The material is used in the manufacture of substrates for printed circuit boards, which experience high mechanical and thermal cyclic loads.

Beryllium oxide (BeO). It has better thermal conductivity than aluminum nitride and better electrical insulation than other ceramic materials for printed circuit board substrates.

Ceramic material is a multiphase system consisting of crystalline, amorphous (glassy) and gas phases. The main one is the crystalline phase, it determines high insulating and other indicators of the product. The glassy phase performs binding functions, provides mechanical strength. The gas phase is pores and microcracks that are formed during the firing process and reduce the mechanical and electrical properties of the material.

Steatite (enstatite) ceramics

Steatite is a ceramic based on natural magnesia (silicate) raw materials, mainly talc ($3MgO{\cdot}4SiO_2{\cdot}H_2O$), and clay components. Dense varieties of talc are called steatite. Steatite (clinoenstatite) ceramics are named after the main crystalline component of this type of ceramics – magnesium metasilicate $MgO{\cdot}SiO_2$ – clinoenstatite.

Magnesium metasilicate forms a number of polymorphic modifications. In addition, a widely occurring phase is known – enstatite (the rest are not found in nature, they exist only in artificial products). To date, there is no consensus in the scientific literature on the phase transformations of magnesium metasilicate.

Advantages of steatite ceramics:

– ch ap material (the basis contains natural raw materials – finely crystalline talc);

– good dielectric properties and high mechanical strength at room and elevated temperatures and in a high-frequency field;

– low abrasiveness, which significantly simplifies the operating conditions of the mold and the process of semi-dry molding of products.

Disadvantages of steatite ceramics:

– narrow intering range (10-30 °C), furnaces with silicon carbide heaters are used;

– aging (de radation of dielectric properties and mechanical strength over time).

Steatite has proven itself in countless areas of application, such as the housing of low-voltage fuses PPN, PN-2 or NH, as a base for halogen lamps, a carrier and holder of heating elements, a crown of gas burners, an insulator, a thermostat housing, etc. [15]. All types of steatite ceramics are characterized by low values of dielectric losses, high mechanical strength, twice as strong as electrical porcelain, and a high value of breakdown voltage. Due to these properties, steatite ceramics are widely used in electrical and radio engineering as high-voltage and high-frequency dielectrics.

Forsterite ceramics

Forsterite is an electronic material based on magnesium orthosilicate Mg_2SiO_4. The developers of this material in Russia are: G.I. Berdov, M.G. Korpachev, A.I. Korpacheva (Novosibirsk), P.G. Usov, V.I. Vereshchagin (Tomsk) et al. Manganese forsterite was developed in Japan. The mineral forsterite is found in nature.

Distinctive features of forsterite densely sintered ceramics:

– high valu s of electrophysical properties;

– incre sed coefficient of linear expansion compared to clinoenstatite ceramics.

Due to the high value of the coefficient of linear expansion, forsterite ceramics are used in vacuum tube technology as an insulator in contact with metals that have a corresponding coefficient of linear expansion. As a result of the absence of polymorphic transformations, forsterite ceramics are not subject to aging. Its main disadvantage is low heat resistance and high TCLE value. Due to this, the products are made in small sizes.

Advantages of forsterite ceramics:

– high m chanical strength;

– high diel ctric properties up to 500 °C;

– the possibil ty of obtaining a vacuum-tight material;

– radiati n-resistant material;

– the possibility of vacuum-tight connection with metallic titanium using active technology (without preliminary metallization);

– simple manufacturing technology using moderate firing temperatures (1350-1380 °C);

– a lower secondary electron emission coefficient than that of alumina ceramics, such as corundum.

Forsterite ceramics are used to manufacture bases of non-wire resistors and as an insulator in contact with metals. Recently, forsterite ceramics have been actively studied as a biocompatible and biodegradable ceramic for the production of bone prostheses. Due to the absence of polymorphic transformations, forsterite is a more promising material in this direction than steatite.

Cordierite ceramics

The MgO-Al_2O_3-SiO_2 system contains cordierite, a ternary crystalline compound with the formula $Mg_2Al_4Si_5O_{18}$, which occurs in nature. Cordierite ceramics are made from natural materials (talc, refractory clays) and artificial ones (alumina, electrofused corundum) [5].

A distinctive property of cordierite ceramics is a low thermal coefficient of linear expansion, due to which cordierite ceramics withstands sharp thermal shocks well, i.e. it is a very heat-resistant material. The high heat resistance of cordierite ceramics allows it to be used in high-voltage and low-voltage electrical engineering, in particular for the manufacture of arc-extinguishing chamber parts in high-voltage switches.

Cordierite ceramics are characterized by a low value of the dielectric loss tangent, equal to 10^{-2}, and a permittivity of 5 at a frequency of 1 MHz. High mechanical strength and chemical resistance allow cordierite to be used as a heat-stable carrier of oxidation-reduction catalysts for automobile exhaust control. Oxygen released from the cordierite surface in the form of anions or in molecular form may participate in catalytic reactions. Cordierite is used as a heat exchanger in gas turbines, as a refractory in industrial furnaces, and in the production of refractory metal coatings. Recently, cordierite has been actively used as a substrate material for integrated circuits and in multilayer low-temperature sintering ceramics (LTCC). Steatite and forsterite are usually white, cordierite can be yellowish due to iron impurities.

High Aluminum Ceramics

Depending on the Al_2O_3-SiO_2 ratio, the following types of high-alumina ceramics are distinguished:

– mullite-siliceous (pre-mullite composition) contains 45-70% Al2O3;

– mullite-corundum (for example, UF-46, UF-53, KM-1, M-4, etc.) contains 70-95% Al_2O_3; the phase composition of the ceramics is determined by the ratio of Al_2O_3 and SiO_2;

– corundum – 95-100% Al_2O_3.

The main component of high-alumina ceramics is aluminum oxide.

The physical and technical properties of high-alumina ceramics with mullite and mullite-corundum crystallization are influenced by the following factors:

– chemical composition, mainly the content of Al_2O_3;

– I_2O_3/SiO_2 ratio and impurity content, as well as introduced additives;

– phase composition and ratio of the main crystalline phases – corundum and mullite, as well as the presence and composition of the glassy phase in the product;

– microstructure of the material - primarily the size and shape of grains, the nature of the distribution of the glassy phase and pores.

High-alumina and corundum ceramics are used as insulators for spark plugs of internal combustion engines, various parts of radio and electrical equipment, insulating ultra-porcelain UF-46 and UF-53.

Advantages of high-alumina ceramics:

– high dielectric properties at room temperature and at elevated temperatures (up to 300 °C);

– high chemical resistance;

– high mechanical strength;

– high heat resistance.

Disadvantages of high-alumina ceramics:

– use of relatively high firing temperatures (for corundum ceramics); narrow sintering range (for UF-46); high abrasiveness (for corundum ceramics).

Piezoceramics

Piezoceramics (ferroelectric ceramic) is an artificial material with piezoelectric and ferroelectric properties, having a polycrystalline structure. Piezoceramics do not belong to the classic types of ceramics, since they do not contain clay. Piezoceramic materials are synthesized from metal oxides. However, the use of a technique characteristic of ceramic technology - firing at a high temperature - justifies the classification of piezoceramics as a ceramic family. "Piezo" (from the Greek "piezo" – to press) indicates that this type of ceramics has a special property – the piezoelectric effect. Compared to single-crystal piezoelectrics, piezoceramics are characterized by their manufacturability, low cost and pronounced piezoelectric and dielectric properties. Piezoceramics can be used to manufacture products of any shape – plates, disks, cylinders, tubes, spheres, etc., which are extremely difficult or impossible to manufacture from single crystals. Piezoceramics are widely used to create acceleration and pressure sensors, shock wave piezoelectric transducers, powerful ultrasound and shock wave emitters, piezoelectric transformers, piezoelectric resonance filters, and delay lines. Piezoceramics are resistant to moisture, mechanical stress, and atmospheric influences.

In terms of physical properties, piezoceramics are polycrystalline ferroelectrics, which are chemical compounds or solid solutions (powders) of grains (crystallites). Crystallite sizes are usually from 2 to 100 μm. Each crystallite is a ferroelectric crystal. Piezoceramics have all the properties inherent in crystalline ferroelectrics. In terms of chemical composition, piezoceramics are complex oxides, usually including divalent lead or barium ions, as well as tetravalent titanium or zirconium ions. By changing the ratios of the starting materials and introducing various additives, piezoceramics compositions with certain electrophysical and piezoelectric characteristics are synthesized. Most piezoceramics compositions are based on chemical compounds with a perovskite-type crystal structure with the formula ABO3 (e.g. $BaTiO_3$, $PbTiO_3$, $LiNbO_3$) and various solid solutions based on them (e.g. $BaTiO_3$ – $CaTiO_3$; $BaTiO_3$ – $CaTiO_3$ – CoCO3; $NaNbO_3$ – $KNbO_3$ systems). Particularly widely used as piezoelectrics are compounds of the lead zirconate titanate system (PZT) $PbTiO_3$ – $PbZrO_3$ (“Piezoelectric ceramics” in the universal encyclopedia of Cyril and Methodius).

The basis of most modern piezoelectric ceramic materials is solid solutions of titanate – lead zirconate (PZT), modified with various components and additives. Piezoceramic materials are also produced based on barium titanate (TB), lead titanate (TS), lead metaniobate (MNS), bismuth titanate (TV), etc.

The first piezoelectric ceramic material was synthesized in 1944 by the Soviet scientist B. M. Vul, who discovered the ferroelectric properties of barium titanate $BaTiO_3$. Almost simultaneously, these properties of barium titanate were discovered by American and Japanese researchers.

In the initial state, the polarization of piezoelectric ceramic elements is zero, since each crystallite is divided into domains and has a random direction of the crystallographic axis. When an external electric field is applied that exceeds a certain value, called a coercive field, the polarization directions of the crystallites are aligned in the direction that is as close as possible to the direction of the polarizing field. Polarized piezoelectric ceramics have pronounced piezoelectric properties.

Depending on the piezoelectric properties, manufacturers divide it into ferroelectric-rigid and ferroelectric-soft. In domestic practice, there is an additional division – ceram cs of medium ferroelectric rigidity. Highly stable, high-temperature, etc. materials are also distinguished.

The value of the piezoelectric modulus d33 reaches several hundred pC/N. Piezoceramics are characterized by high values of relative permittivity. The quality of piezoceramics is characterized by the following main parameters accepted abroad:

K^T_{33} (e^T_{33}/e_0) – relative permittivity;
tg d – dielectric loss tangent at 1 kHz in weak fields;
T_c (T_k) – Curie point temperature;
K_p K_{33} K_{31} K_{15} – electromechanical coupling coefficients;
d_{33} -d_{31} d_{15} – piezoelectric moduli;
g_{33} g_{31} g_{15} – electrical voltage coefficients;
Y^E_{11} Y^E_{33} – Young's moduli;
N_L N_T N_R – frequency constants;
S^E_{11} S^E_{33} – elasticity parameter;
r – density;
Q_m – mechanical quality factor.

A composite may have a ceramic, metal or polymer matrix.

The continuous phase, which usually has a higher proportion in the volume of the composite material, is called the matrix. The second component is called a filler or reinforcing phase, the role of which is often to increase the mechanical properties of the matrix (Table 2).

The principle of chemical and physical compliance is the absence of degradation of the matrix properties due to contamination with foreign chemical elements or the formation of defects that worsen the functional properties (mutual chemical inertness, absence of phase transitions, compliance of thermal expansion coefficients, as well as: microparticles and globules in the matrix, layered composites, reinforcing threads, three-dimensional mesh, etc.).

Table 2

Matrix	Filler	Properties
Polymers	Fiberglass	High strength
Carbon	Carbon fiber	Low density, high thermal conductivity, fire resistance (~2000 °C)
Metal	Metal oxide	Dispersion hardening
Metal	Ceramics (cermets)	Heat resistance, hardness
Ceramics	Metal (ultracermets)	Increased strength, thermal conductivity
Al_2O_3	Cr, W-Cr	Gas turbines
TiC	Ni, Cr	Wear resistance
ThO_2	Mo	Emission cathodes
Ceramics	Ceramics	Pinning, refractories

Distinctive properties of composites:

1. Consist of two or more phases that differ in their chemical and mineral compositions; the phases are separated by a clearly defined boundary;
2. The materials acquire new properties that differ from the properties of their constituent components;
3. The materials are heterogeneous in the nano- and micrometer size range (up to 500 μm), but are fairly homogeneous in terms of macroscopic characteristics (density, hardness, color);
4. The composition, shape, and distribution of the material components are designed in advance;

5. The properties of the material are determined by each of its components.

The main stages of obtaining ceramic products:

• sorting and cleaning from impurities;
• grinding and mixing according to a given recipe with the addition of water;
• forming parts by pressing, stamping;
• drying and firing in kilns.

Advantages: high heat resistance and mechanical strength, high radiation resistance, resistance to aging, obtaining specified characteristics by changing the composition of the mass, non-hygroscopic and weather-resistant.

Disadvantages: impossibility of obtaining thin flexible products, difficulty of mechanical processing (products can only be ground), porosity.

According to their purpose, they are divided into three groups: insulator, capacitor and ferroelectric ceramics.

Porcelain is the oldest type of ceramics used as an insulating material. Porcelain is used at low frequencies, at low voltages as an insulating and structural material. The raw material is high-quality clay – kaolin (approximately 50%), quartz sand (approximately 25%) and feldspar (approximately 25%). Porcelain is used to make resistor and connector housings, lamp panels. At high voltages, porcelain is used to manufacture terminals of high-voltage equipment and insulators of overhead lines (Fig. 1).

Fig. 1. Insulating ceramics

Ceramic capacitor materials differ from ceramic insulator materials by a higher dielectric constant, which allows them to be used to manufacture ceramic capacitors of large capacity and relatively small dimensions. Ceramic capacitors are not hygroscopic and do not require protective housings and shells, which are necessary for paper and mica capacitors (Fig. 2).

Ceramic capacitors are manufactured using ceramic technology methods – casting in plaster or steel molds, and then fired in furnaces at a temperature of 1450-1700º.

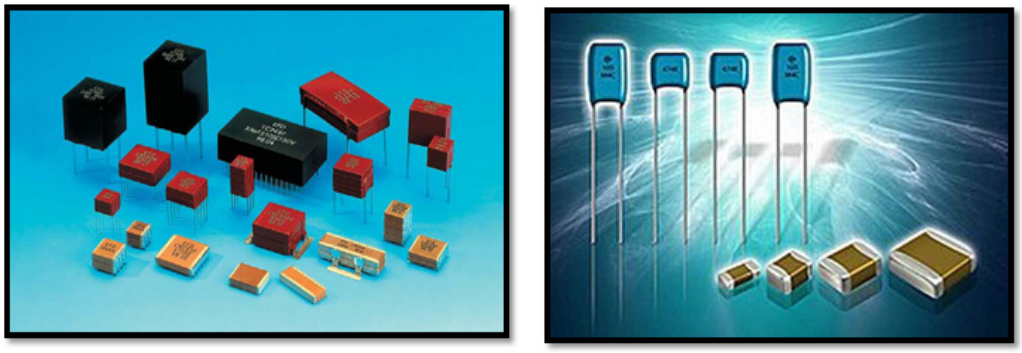

Fig. 2. Ferroelectric ceramics

Ferroelectric ceramic materials (ferroelectric ceramics) have abnormally high values of permittivity, which allows them to be used as temperature sensors when changing it by electrical methods. The high permittivity of ferroelectric dielectrics allows them to be used to manufacture miniature electric capacitors of large capacity. The permittivity of ferroelectric dielectrics increases significantly with the growth of the voltage applied to them, which is not observed in conventional dielectrics. This characteristic property is used in dielectric amplifiers. All ferroelectric dielectrics have characteristic properties only up to a certain temperature. When these temperatures are exceeded, they lose their properties and become conventional dielectrics.

Conclusion

The development of radio electronics at the present stage, increasing reliability, reducing the dimensions and weight of devices are closely related to the development, study of properties and application of new materials. These include new ceramic and composite materials that can withstand high temperatures and successfully operate in aggressive environments.

Ceramic materials are very diverse, each of them has its own unique chemical properties. They are very widely used in radio electronics and are promising for the development and improvement of designs of radio electronic devices.

Currently, industrial progress requires electronics to constantly increase the level of power, efficiency, reliability and durability. For modern devices, in particular powerful RF and microwave transmitters, power transistors, power converters, reliability under high currents and high temperatures is certainly a key factor.

REFERENCES

[1] A. S. Tolkacheva, I. A. Pavlova, “Technology of ceramics for materials of the electronics industry,” In 2 parts. Part 1. Ekaterinburg: Publishing house of the Ural. University, 2019. 124 p. ISBN 978-5-7996-2682-2.

[2] J. Zhu et al., “Study on Properties of Lanthanum Doped SrBi4 Ti4 O15 and Sr2 Bi4 Ti5 O18 Ferroelectric Ceramics,” *Jpn. J. Appl. Phys*. 2003. Vol. 42, pp. 5165-5168.

[3] B. A. Rotenberg, “Ceramic capacitor dielectrics: a monograph,” St. Petersburg: Printing house of OAO Research Institute Girikond, 2000. 246 p.

[4] Chemical technology of ceramics: a textbook. Moscow: Stroymaterialy, 2003. 496 p.

[5] E. G. Avakumov, A. A. Gusev, “Cordierite – a promising ceramic material,” Novosibirsk: Publishing house of the Siberian Branch of the Russian Academy of Sciences, 1999. 166 p.

[6] P. V. Zaenchkovsky, O. Yu. Makarov, “Prospects for the use of ceramic materials in the radio-electronic industry,” *Bulletin of the Voronezh State Technical University*. 2009, pp. 20-24.

[7] M. T. Sebastian, R. Ubik, H. Jantunen, “Low-loss dielectric ceramic materials and their properties,” *Int. Mater. Rev*. 2015. No. 60, pp. 392-412. doi: 10.1179/1743280415Y.0000000007

[8] I. M. Rini, D. Iddles, “Microwave dielectric ceramics for resonators and filters in mobile communication networks,” *J. Am. Ceram. Soc*. 2006. No. 89, pp. 2063-2072. doi: 10.1111/j.1551-2916.2006.01025.x
[9] Y. Bai, J. Varghese, M. T. Sebastian, “Dielectric ceramics for electronic applications,” *Front. Mater*. 2021. No. 8. P. 714522. doi: 10.3389/fmats.2021.714522
[10] D. Yakovlev, “Production of printed circuit boards from multilayer ceramics,” *Production technologies*. 2020. No. 5 (00196), pp. 138-142. DOI: 10.22184/1992-4178.2020.196.5.138.142
[11] A. P. Kazantsev, “Materials and components of radio electronics,” Minsk: Belarusian State University of Informatics and Radioelectronics, 2004. 142 p.
[12] M. A. Vartanyan, E. S. Lukin, N. A. Popova, “New generation ceramic materials for electronic devices,” *Advances in chemistry and chemical technology*. 2008. Vol. 22. No. 7 (87), pp. 7-10.
[13] Z. Koryakova, “Ceramic materials in microwave technology,” *Components and technologies*. 2011. No. 5 (118), pp. 184-186.
[14] A. Fontana et al., "A Novel Approach Toward the Integration of Fully 3-D Printed Surface-Mounted Microwave Ceramic Filters," in IEEE Transactions on Microwave Theory and Techniques, vol. 71, no. 9, pp. 3915-3928, Sept. 2023, doi: 10.1109/TMTT.2023.3267541.
[15] A. Maksimov, “Ceramic materials for IC and semiconductor device cases,” *Components and technologies*. 2011. No. 5 (118), pp. 188-190.
[16] K. E. Lukyashin, V. V. Osipov, V. A. Shitov, R. N. Maksimov, V. V. Platonov, I. V. Solomonov, A. V. Ishchenko, “New highly transparent ceramic materials,” *Rocket and space technology*. 2016. Vol. 1. No. 2 (8). P. 9.